Title

Eosinophils regulate adipose tissue inflammation and sustain physical and immunological fitness in old age

Journal

Nature Metabolism, 2(8)

ISSN

2522-5812

Authors

Brigger, Daniel
Riether, Carsten
van Brummelen, Robin
et al.

Publication Date

2020-08-01

DOI

10.1038/s42255-020-0228-3

Peer reviewed

HHS Public Access

Author manuscript

Nat Metab. Author manuscript; available in PMC 2021 February 01.

Published in final edited form as:

Nat Metab. 2020 August ; 2(8): 688–702. doi:10.1038/s42255-020-0228-3.

Eosinophils regulate adipose tissue inflammation and sustain physical and immunological fitness in old age

Daniel Brigger[1,2], **Carsten Riether**[3,4], **Robin van Brummelen**[1,2], **Kira I. Mosher**[5,†], **Alicia Shiu**[5,†], **Zhaoqing Ding**[5,†], **Noemi Zbären**[1,2], **Pascal Gasser**[1,2], **Pascal Guntern**[1,2], **Hanadie Yousef**[5], **Joseph M. Castellano**[6], **Federico Storni**[1,2], **Neill Graff-Radford**[7], **Markus Britschgi**[5,†], **Denis Grandgirard**[8], **Magdalena Hinterbrandner**[3,4], **Mark Siegrist**[2], **Norman Moullan**[9], **Willy Hofstetter**[2], **Stephen L. Leib**[8], **Peter M. Villiger**[1,2], **Johan Auwerx**[9], **Saul A. Villeda**[10], **Tony Wyss-Coray**[5,11], **Mario Noti**[12,†,*], **Alexander Eggel**[1,2,*]

[1]Department of Rheumatology, Immunology and Allergology, University Hospital, University of Bern, Bern, Switzerland. [2]Department for BioMedical Research, University of Bern, Bern, Switzerland. [3]Tumor Immunology, Department of Clinical Research, University of Bern, Bern, Switzerland. [4]Department of Medical Oncology, Inselspital, Bern University Hospital, University of Bern, Switzerland [5]Department of Neurology and Neurological Sciences, Stanford University School of Medicine, Stanford, California, USA. [6]Department of Neurology, Icahn School of Medicine at Mount Sinai, New York, NY 10029, USA [7]Department of Neuroscience, Mayo Clinic, Jacksonville, Florida, USA. [8]Institute for Infectious Diseases, University of Bern, Bern, Switzerland [9]Laboratory of Integrative and Systems Physiology, École Polytechnique Fédérale de Lausanne, Lausanne, Switzerland. [10]Department of Anatomy, University of California San Francisco, San Francisco, California, USA. [11]Center for Tissue Regeneration, Repair, and Restoration, VA Palo Alto Health Care System, Palo Alto, California, USA. [12]Institute of Pathology, Division of Experimental Pathology, University of Bern, Bern, Switzerland.

Abstract

Adipose tissue eosinophils (ATE) are important for the control of obesity-associated inflammation and metabolic disease. However, how aging impacts the regulatory role of ATEs remains unknown. Here, we show that ATEs undergo significant age-related changes in distribution and function associated with impaired adipose tissue homeostasis and systemic low-grade inflammation in both humans and mice. We find that exposure to a young systemic environment

Correspondence to: Alexander Eggel, PhD, Department of Rheumatology, Immunology and Allergology, University of Bern, CH-3008 Bern, Switzerland, alexander.eggel@dbmr.unibe.ch, Mario Noti, PhD, Nestlé Research, Department of Gastrointestinal Health Immunology, CH-1000 Lausanne, Switzerland, mario.noti@rd.nestle.com.

Author contributions: M.N. and A.E. designed the project. D.B., C.R., R.v.B., K.I.M., A.S., Z.D., N.Z., P. Ga., P.Gu, H.Y., J.M.C., M.B., M.H., D.G., M.S., N.M., S.A.V., M.N. and A.E. performed the experiments. F.S. and N.G.R. provided human samples. W.H., S.L.L., P.M.V., J.A., S.A.V. and T.W.C. provided important advice. D.B., M.N. and A.E. analyzed the data and wrote the manuscript.

[†]Present addresses: Department of Chemical and Biological Engineering, University of California, Berkeley, USA (K.I.M.); Amplitude Analytics Inc., San Francisco, California, USA (A.S.); Johnson & Johnson Pharmaceutical Research & Development, L.L.C., San Diego, California, USA (Z.D.); Roche Pharma Research and Early Development, Neuroscience Discovery, Roche Innovation Center Basel, F. Hoffmann-La Roche Ltd, Grenzacherstr. 124, 4070 Basel, Switzerland (M.B.). Nestlé Research, Department of Gastrointestinal Health, Immunology, 1000, Lausanne, Switzerland (M.N.)

[*]Authors contributed equally to this work.

Competing interests: The authors declare no competing interests.

partially restores ATE distribution in aged parabionts and reduces adipose tissue inflammation. Approaches to restore ATE distribution using adoptive transfer of eosinophils from young mice into aged recipients proved sufficient to dampen age-related local- and systemic low-grade inflammation. Importantly, restoration of a youthful systemic milieu by means of eosinophil transfers resulted in systemic rejuvenation of the aged host manifesting in improved physical and immune fitness that was partially mediated by eosinophil-derived IL-4. Together, these findings support a critical function of adipose tissue as a source of pro-aging factors and uncover a novel role of eosinophils in promoting healthy aging by sustaining adipose tissue homeostasis.

White adipose tissue (WAT), besides its established role in nutrient sensing and energy storage, is a highly active endocrine organ that undergoes significant changes in distribution and function with progression of age[1]. Emerging studies suggest that the development of frailty and age-related morbidities is accelerated by the loss of WAT homeostasis, while strategies that delay or limit WAT dysfunction have been shown to enhance health- and lifespan across species[2–12]. WAT is home to a dense network of immune cells including lymphocytes, group-2 innate lymphoid cells, macrophages and eosinophils which have the capacity to regulate tissue homeostasis and metabolism[13]. While eosinophils are well known for their cytotoxic effector functions in allergic responses and host protection against parasite infections[14], recent studies have emphasized the importance of adipose tissue eosinophils (ATEs) in the maintenance of alternatively activated adipose tissue macrophages (ATMs) and the control of obesity-associated WAT inflammation in metabolic disease[15,16]. While obesity and aging share numerous biological similarities related to WAT dysfunction[17], it remains to be determined whether ATEs can regulate WAT homeostasis and organismal health in old age. Here, we identify WAT as a source of the pro-aging factor CCL11[18], a potent chemoattractant for eosinophils, which accumulates systemically with age and negatively correlates with ATE distribution in humans and mice. These age-related changes were closely associated with WAT dysfunction and systemic low-grade inflammation, two significant risk factors for both morbidity and mortality in the elderly[1,19,20]. We find that eosinophils from young organisms preferentially migrate to WAT of aged mice, restore WAT function and dampen systemic low-grade inflammation partially mediated by eosinophil-derived IL-4. Importantly, restoration of a youthful environment by means of eosinophil transfers translated into systemic rejuvenation of the aged host supporting a previously unrecognized role of eosinophils in promoting healthy aging.

Age-related changes in the systemic environment partially originate in WAT

To identify soluble blood factors that accumulate with age, we employed a proteomic approach to measure 170 hormones, cytokines, chemokines and other secreted signaling proteins in plasma of aging humans and mice (Supplementary Table 1 and 2). Analysis of the 67 and 51 detectable factors (Supplementary Table 3) in human and mouse plasma, respectively, revealed a clear blood-based systemic aging signature (Fig. 1a and b). Unsupervised clustering of normalized mean protein levels separated sample groups according to age in both species. Furthermore, we identified nine plasma proteins among a total of 41 overlapping factors that significantly correlate with age in humans and mice (Fig. 1c, Supplementary Table 4). Consistent with previous studies[18], we find that CCL11

(Eotaxin-1) and CCL2 (MCP-1) rank amongst the top age-correlating factors (Supplementary Table 5) in plasma of both humans (Fig. 1d, e) and mice (Fig. 1 f, g) with absence of sex-specific differences. To determine the biological origin of increased systemic CCL11 and CCL2 levels we performed tissue screens in aged mice. Among 12 tissues assessed and consistent with previous reports[21] WAT represents a major source of CCL11 and CCL2 (Extended Data Fig. 1a–d) which significantly increase with age (Extended Data Fig. 1e, f).

Age-related WAT inflammation is associated with altered adipose tissue eosinophil distribution

Given that the pro-aging factor CCL11 is a potent chemoattractant for eosinophils, we next assessed eosinophil distribution in visceral WAT. Using histological and flow cytometric approaches, we identified the presence of adipose tissue eosinophils (ATEs) in both humans (Fig. 2a–d, Extended Data Fig. 2a and Supplementary Table 6) and mice (Fig. 2g, h and Extended Data Fig. 2d). Despite the observed age-related increase of CCL11 levels in WAT we find an inverse correlation with ATE frequencies (Fig. 2e, i), while absolute numbers remain unchanged (Extended Data Fig. 2e). In contrast, but consistent with an age-related increase in WAT CCL2 levels, both frequencies and numbers of ATMs increase with age (Fig. 2i and Extended Data Fig. 2e) resulting in a significantly lower ATE to adipose tissue macrophage (ATM) ratio in WAT of aged compared to young mice. Reduced ATE frequencies in aged humans and mice were further associated with visceral adipose tissue inflammation apparent by a significant increase in *Il6* and *Il1β* (Fig. 2f, j) and adipocyte hypertrophy (Extended Data Fig. 2b–c, f-g). These data suggest that age-related changes in systemic CCL11 and CCL2 levels and associated alterations in ATE distribution are conserved in both humans and mice and may contribute to WAT dysfunction in old age.

Exposure to a young systemic environment restores ATE:ATM ratios and limits WAT inflammation

Given the rejuvenating potential of a youthful environment on muscle, bone, heart, brain and CNS[22–27], we next assessed whether exposure of aged mice to a young circulation has the potential to restore WAT homeostasis. To do so, we took advantage of heterochronic parabiosis[28], a model system in which two animals of different age are joined in order to share a common circulatory system (Fig. 3a). In line with reduced ATE and increased ATM frequencies in aged mice (Fig. 2i), we observed similar changes in old isochronic parabionts (Fig. 3b, c). Strikingly, exposure to a young systemic milieu resulted in partial restoration of ATE:ATM ratios in WAT of old heterochronic parabionts compared to old isochronic controls (Fig. 3 b, c). To assess whether the changes in ATE:ATM ratios are due to homing of young eosinophils into old WAT, we paired young GFP-reporter mice to either young or aged wild-type mice through parabiosis (Fig. 3e) and assessed frequencies of GFP-positive eosinophils in WAT. Employing this model system, we found GFP-positive eosinophils in WAT of old heterochronic wild-type mice, indicating that eosinophils from young parabionts efficiently migrate into WAT of their aged partners (Fig. 3f, g). We further observed similar percentages of GFP-negative eosinophils in the WAT of young isochronic and heterochronic

GFP-reporter mice (Fig. 3f, g), implying that eosinophils from the old parabiont retain their migratory capacity when exposed to a young systemic environment. Given reported immuno-regulatory properties of eosinophils in WAT[15,29,30], we next assessed whether restoration of ATE:ATM ratios in old heterochronic mice was associated with alterations in adipose tissue inflammation. Strikingly, expression levels of *Il6, Ccl2* and *Il1b* in WAT of old heterochronic parabionts were significantly reduced compared to old isochronic mice (Fig. 3d). Collectively, these data indicate that age-related changes in ATE:ATM ratios and associated WAT inflammation can be partially restored by exposure to a youthful systemic environment.

Transferred eosinophils predominantly home to WAT and reduce local and systemic inflammation.

To assess whether restoration of ATEs is sufficient to resolve aging signatures in WAT, we transferred eosinophils from young mice into aged recipients. Owing to the limiting numbers of eosinophils in wild-type mice, we used sort-purified eosinophils from IL-5 transgenic mice (C57BL/6J-Tg(Il5)1638Jlee)[31] for adoptive transfers. In a first approach, we adoptively transferred sort-purified IL-5 transgenic GFP^+ eosinophils to aged recipients to assess tissue distribution and surface marker phenotype of transferred cells (Fig. 4a and Extended Data Fig. 3a and b). Among 11 tissues assessed we find that transferred eosinophils predominantly home to WAT of aged mice (Fig. 4 a and b) with no alterations in Siglec-F surface expression compared to WAT resident endogenous eosinophils (Extended Data Fig. 3c–e). Given preferential homing of transferred eosinophils to WAT, we next assessed whether a prolonged protocol of eosinophil transfers to aged mice has functional consequences for age-related WAT dysfunction. To do so, aged mice were injected twice a week for 4 consecutive weeks with either PBS control (Aged-PBS), eosinophils (Aged-yEOS) or control granulocytes (Aged-yNEU) from young donors (Fig. 4c and Extended Data Fig. 4a). Flow cytometric analyses confirmed preferential homing of transferred eosinophils to WAT resulting in the restoration of ATE:ATM ratios in aged recipients (Fig. 4d), while no changes in ATE:ATM ratios in mice transferred with control granulocytes were observed (Extended Data Fig. 4b). Consistent with observed changes in ATE:ATM ratios and the reduction of WAT inflammation in old heterochronic parabionts, the levels of pro-inflammatory mediators IL-6, CCL2 and IL-1β were significantly reduced in WAT of Aged-yEOS compared to Aged-PBS mice (Fig. 4 e). Additionally, Aged-yEOS mice showed a significant reduction in age-related adipose tissue hypertrophy (Extended Data Fig. 2f, g) indicating that transferred eosinophils have the capacity to control age-related WAT dysfunction. No such changes in response to eosinophil transfers were observed in subcutaneous adipose tissue (Extended Data Fig. 5a–e) nor did transfer of a control granulocyte population affect age-related WAT parameters (Extended Data Fig. 4c). Further, reduced WAT inflammation in Aged-yEOS mice correlated with decreased systemic plasma levels of IL-6, CCL2 and IL-1β (Fig. 4f) supporting the hypothesis that aging visceral WAT may represent an important source of pro-inflammatory mediators that fuel systemic low-grade inflammation and aging phenotypes.

Many of the immune-regulatory properties of ATEs have been attributed to their production of IL-4[15]. To assess whether the observed reduction in local and systemic low-grade inflammation in response to eosinophil transfers is regulated through eosinophil-derived IL-4, we transferred IL-4-deficient eosinophils derived from IL-5 transgenic young mice into aged recipients (Aged-yEOS$^{IL4-/-}$). Both transfer of IL-4 sufficient and deficient eosinophils restored ATE:ATM ratios (Fig. 4d) with eosinophil-derived IL-4 being sufficient to reduce local and systemic age-related increases in IL-6, CCL2 and IL-1β when compared to Aged-PBS controls (Fig. 4e, f). Inter-group comparisons between Aged-yEOS and Aged-yEOS$^{IL4-/-}$ showed significance for IL-6, but not CCL2 and IL-1β (data not shown). While adipose tissue eosinophils (ATE) have been reported to control obesity-associated WAT inflammation and metabolic disease, restoring ATEs in aged mice by means of adoptive eosinophil transfers from young donors did not alter glucose metabolism (Extended Data Fig. 6a and b). Together, these data indicate that transfer of eosinophils from young donors reduce age-related WAT dysfunction and systemic low-grade inflammation in aged recipients, a mechanism that is in part regulated via eosinophil-intrinsic IL-4.

Eosinophils from young donors improve physical fitness in aged hosts

The activity pattern of aging organisms continuously decreases as they become sedentary with widespread consequences for WAT distribution and function[32]. To assess whether improved WAT homeostasis and the associated decrease in systemic inflammation in Aged-yEOS mice translates into improved physical fitness, we performed voluntary and forced physical exercise tests. No changes in voluntary activity were apparent between the different groups (Extended Data Fig. 7a and b). While we observed a significant age-related loss of forced physical performance between Young and Aged-PBS treated mice (Fig. 5 a and b, e and f), the comparison of pre- to post-transfer measurements in maximal force (grip strength) and endurance tests (rotarod) revealed significant intra-individual improvements in Aged-yEos mice but not in Aged-PBS controls or Aged-yEOS$^{IL4-/-}$ littermates (Fig. 5c and g). Further, inter-group comparison showed significant physical improvements in both tests exclusively in Aged-yEOS mice, highlighting a rejuvenating potential of IL-4 competent eosinophils in aged hosts (Fig. 5d and h). No alterations in both voluntary and forced physical tests were observed in aged mice transferred with a control granulocyte population (Aged-yNEU) (Extended Data Fig. 4d, Extended Data Fig. 7). The fact that Aged-yEOS mice showed increased physical fitness over aged-PBS controls suggests that transfer of eosinophils to aged hosts may have a direct effect on muscle function. To test this hypothesis, we quantified muscle stem cells (satellite cells) from the hind limbs reported to progressively decrease with age[33]. Although eosinophil transfers into aged mice partially restored an age-related decrease in muscle stem cells, no changes in muscle mass, fiber size, number of centrally nucleated myofibers and *ex vivo* myogenic potential of muscle stem cells were measured (Extended Data Fig. 8a–g). In addition to the low number of transferred eosinophils in muscle tissue (Fig. 4b) these data indicate that improvement in physical fitness observed in Aged-yEOS mice is likely mediated through indirect effects.

Despite the fact that eosinophils do not carry the IL-5 transgene alterations in gene expression profiles of eosinophil progenitors derived from transgenic and wild-type mice have been reported[34]. To assess whether eosinophils from wild-type mice might have similar

rejuvenating effects on aged mice, we generated bone marrow (BM) derived eosinophils (BMDE) from young wild-type mice for subsequent adoptive transfer experiments (Extended Data Fig. 4h). Consistent with results obtained with eosinophils derived from IL-5tg mice (eosinophils do not express the transgene), wild-type BDMEs were sufficient to restore ATE:ATM ratios, dampen WAT and systemic IL-6 concentrations and improve physical fitness in aged mice (Extended Data Fig. 4i–m). Together these data indicate that eosinophils derived from both IL-5 transgenic mice and wild-type donors have the potential to improve age-related deterioration of physical fitness.

Homing of adoptively transferred eosinophils to WAT is required to improve physical fitness in aged hosts

Next, we assessed whether homing of adoptively transferred eosinophils to WAT of aged mice is required for the observed reversal of aging signatures. Previous studies reported the efficacy of pertussis toxin (PT) to inhibit migration of eosinophils from BM to peripheral tissues[35]. Adopting a similar approach, sort-purified and CSFE-labeled IL-5 transgenic eosinophils were pre-treated *ex vivo* with a concentration of PT not affecting survival prior to transfer into aged mice (Aged-yEOS^{PT}) (Fig. 6a). This treatment regimen significantly inhibited eosinophil homing to WAT (Fig. 6b). Consistent with impaired homing to WAT, repetitive transfer of PT pre-treated eosinophils to aged mice failed to recapitulate beneficial effects on WAT inflammation and physical fitness of vehicle-treated eosinophils (Fig. 6c–h). Together, these data indicate that eosinophils have the potential to improve age-related deterioration of physical fitness by reducing WAT inflammation, a process that is mediated through homing of transferred eosinophils to WAT.

Systemic IL-6 neutralization partially phenocopies eosinophil-induced amelioration of physical fitness

Our data suggest that reducing systemic low-grade inflammation by means of eosinophil transfers to aged hosts is sufficient to reverse age-related declines in physical fitness. To further test this hypothesis, we targeted systemic IL-6 in aged mice by means of blocking antibodies, one of the key cytokines associated with inflamm-aging that was significantly reduced upon eosinophil transfers to aged mice. To do so, aged mice were injected with an IL-6-blocking antibody (Aged-aIL6) or isotype control (Aged-ISO) over a 4 week period (Fig. 6i). The used treatment regimen resulted in a significant reduction in plasma IL-6 levels in Aged-aIL6 mice compared to the Aged-ISO group (Fig. 6j). Importantly, blocking systemic IL-6 responses in aged mice phenocopied the rejuvenating effects observed in Aged-yEOS mice in physical endurance tests (Fig. 6k and l). However, compared to Aged-yEOS mice (Fig. 4e, f), intra-individual improvents in strength tests in Aged-aIL-6 mice did not show a positive difference (Fig. 6m and n) suggesting that anti-IL6 treatment does not rejuvenate, but rather halt an age-related progressive decline in muscle strength. Thus, IL-6 may represent one of multiple factors contributing to systemic inflamm-aging and associated age-related declines in physical fitness.

Eosinophils from young donors restore age-related myeloid skewing of the HSPC lineage

To test another compartment known to progressively lose its function with age, we investigated the impact of eosinophil-mediated reduction in systemic low-grade inflammation on bone marrow hematopoiesis of aged mice. While hematopoiesis is tightly balanced in young mice, hematopoietic stem/progenitor cells (HSPC) are skewed towards the myeloid lineage with progression of age[36,37]. Previous studies have reported a key role of age-related pro-inflammatory mediators such as IL-6, IL-1β and TNFα in this reprogramming of HSPCs[38–41]. Given that transfer of eosinophils from young mice to aged recipients resulted in a reduction of local and systemic inflammation, we next investigated the composition and differentiation potential of HSPC in BM of young, aged- and aged-intervention groups. In line with previous reports the number of LSKs and HSCs (HSC-AD and HSC-SLAM) were elevated in aged mice compared to young controls (Fig. 7a–c)[42]. While Aged-yEOS mice showed a significant reduction in absolute numbers in HSCs compared to the Aged-PBS group, no significant changes were observed in Aged-yEOS$^{IL4-/-}$ mice (Fig. 7a–c). Along with a decrease in HSPCs in Aged-yEOS mice, absolute numbers of all HSPC sub-populations (CLPs, CMPs and GMPs) were also reduced (Extended Data Fig. 9a–c). Importantly, Aged-yNEU control mice did not show any changes in HSCs and HSPC subsets and the corresponding sub-populations as compared to the Aged-PBS group (Extended Data Fig. 4e, f). To assess whether the observed changes in HSPC numbers in Aged-yEOS mice determined by phenotypic analysis also translate into functional alterations, we plated BM cells from Aged-PBS, Aged-yEOS and Aged-yEOS$^{IL4-/-}$ mice in methylcellulose cultures and assessed colony formation *in vitro*. HSPCs from aged mice are known to generate increased proportions of monocyte CFUs[43]. Strikingly, Aged-yEOS but not Aged-yEOS$^{IL4-/-}$ mice showed significant reduction in myeloid colony-forming units (CFUs) over Aged-PBS controls (Fig. 7d), indicating that eosinophils can partially reverse age-related myeloid skewing in part through an IL-4 dependent manner. To investigate the *in vivo* sustainability of the eosinophil-mediated hematopoietic changes, we generated mixed BM chimeras by transferring whole BM of Young, Aged-PBS or Aged-yEOS mice (Ly5.2) together with a young congenic competitor BM (Ly5.½) into lethally irradiated recipient mice (Ly5.1) (Fig.7e). Flow cytometric analysis of peripheral blood (Fig. 7f, g) revealed a decrease in myeloid output in mice receiving BM of Aged-yEOS mice as compared to Aged-PBS bone marrow transplants (Fig. 7h). However, this effect was transient and disappeared over time. In line with these findings, analysis of BM revealed that mice transplanted with BM from Aged-yEOS mice had comparable HSC numbers to mice receiving Aged-PBS BM 16 weeks after transplantation. In contrast, mice transplanted with BM from young mice had significantly decreased HSC numbers compared with mice receiving BM from Aged-PBS mice (Fig. 7i). Together, our data demonstrate that eosinophils from young donors have the potential to transiently restore age-biased HSPC numbers and reverse myeloid skewing partially mediated by eosinophil-derived IL-4.

Eosinophils from young donors boost immunological fitness in old age

Age-related changes in HSPC function contribute to poor vaccination responses and increased susceptibility to infections[44–46]. To study functional consequences of an altered hematopoietic stem cell pool in Aged-yEOS mice, we assessed immunological fitness of aged mice in response to immunization. Young, Aged-PBS, Aged-yEOS and Aged-yEOS$^{IL4-/-}$ mice were immunized with ovalbumin (OVA) (Fig. 8a). Upon secondary immunization, splenic PNA-positive germinal center B-cells (GCBs) were quantified using a flow cytometric approach (Fig. 8b and Extended Data Fig. 9d). We find decreased numbers of splenic antigen-specific germinal center B-cells in Aged-PBS compared to Young mice after immunization. This age-related decline was restored in the Aged-yEOS and to a lesser extent in the Aged-yEOS$^{IL4-/-}$ group with no intergroup significance (Fig. 8b, c). Similar results were obtained using an OVA-specific IgG ELISpot assay with splenocytes. While spleens of Aged-PBS mice harbored significantly less OVA-specific IgG producing B-cells than their young counterparts, transfer of IL-4 competent eosinophils into aged mice partially restored these numbers (Fig. 8d, e). Consistent with ELISpot data, total OVA-specific IgG serum titers were significantly elevated in Aged-yEOS mice as compared to Aged-PBS (Fig. 8f). These data demonstrate that the observed age-related decline in immunization responses is plastic and can be partially reversed by adoptive transfer of eosinophils from young donors. In summary, our results demonstrate that transfers of eosinophils from young donors into aged hosts partially restore the hematopoietic stem cell pool and improve age-related immune cell dysfunction and immunological fitness.

Discussion

To our knowledge, this study collectively provides the first demonstration that dysregulated eosinophil responses in WAT represent a conserved aging phenotype in humans and mice. We find that restoration of adipose immune homeostasis by transfer of eosinophils from young mice reduces subclinical low-grade inflammation with widespread rejuvenating consequences for the aging host. We demonstrate that young donor eosinophils reduce WAT and systemic low-grade inflammation, restore age-related myeloid skewing, improve physical fitness and boost immune responsiveness to immunization.

The perception of WAT and its physiological role has considerably changed over the last decade. Initially identified as an inert fat depot and energy reservoir it is now recognized as an important endocrine immune organ fulfilling important metabolic tasks[47]. Lately, WAT has gained increasing attention as a biological driver of aging and associated functional declines[48–50]. Various studies have highlighted aging WAT as a major source of pro-inflammatory mediators[13,51] and gene-expression databases of aging tissues confirm these findings[21]. Given that WAT is physically connected to virtually all organs its age-related changes seem critical for the observed system-wide pathophysiology. This hypothesis has been supported by many studies demonstrating that reduction of WAT mass and dysfunction by means of exercise, caloric restriction, senolytics or bariatric surgery extend health- and lifespan in various organisms[2–12]. Our data highlight that restoring WAT dysfunction by adoptive transfers of eosinophils from young donors to aged recipients improves pre-existing aging phenotypes including frailty and immunosenescence (Fig.9). Given the conserved age-

related decline in ATEs in humans, our findings may have broad clinical implications and thus help to identify novel anti-aging strategies specifically targeting WAT.

Inflamm-aging describes the age-related increase in systemic low-grade chronic inflammation, which has been suggested to represent a common link in age-related diseases[20,52]. While there is a vast amount of literature on the direct contribution of WAT to systemic low-grade inflammation in obesity[53], direct evidence for aging WAT as a main driver of inflamm-aging is enigmatic and scarce. However, obesity and aging share many aspects related to dysfunctional WAT physiology[17]. Our findings that a reduction in inflammatory markers in WAT upon eosinophil transfers (e.g. IL-6, CCL2 and IL-1β) translates into reduced chronic low-grade inflammation provides further indirect evidence that WAT may represent an important source of pro-aging factors. To test whether bypassing the eosinophil transfer approach and directly targeting down-stream inflammatory mediators that were found to be significantly changed upon eosinophil transfers will result in similar rejuvenating effects, we used a protocol to deplete systemic IL-6. Importantly, previous work has demonstrated that systemic accumulation of IL-6 is not only a biomarker of aging but also promotes age-related frailty[54,55]. Our approach blocking systemic IL-6 in aged mice confirms its pro-aging properties in that we observed a halting or even partial reversal of the age-related decline in physical performance.

Our findings highlight that transferred eosinophils efficiently migrate to WAT to restore age-related WAT dysfunction resulting in reduced systemic low-grade inflammation and improved physical and immunological fitness. Importantly, homing of eosinophils to WAT was a prerequisite for the observed systemic rejuvenation of the aged host, as blocking of eosinophil migration to WAT by means of pertussis toxin treatment failed to reproduce beneficial effects on WAT homeostasis and age-related physical deterioration. Together, these findings identify a direct link between eosinophil homing to WAT and improvements in physical fitness.

While reducing systemic low-grade inflammation by means of adoptive eosinophil transfers to aged mice resulted in improved physical performance, our findings do not support a direct effect of eosinophils on muscle function. Despite a significant increase in muscle stem cell numbers in response to eosinophil transfers no changes in muscle mass and fiber size were observed in aged recipients. Thus, the rejuvenating potential of transferred eosinophils for physical performance of aged recipients may rather be explained by the reduction of systemic low-grade inflammation and associated improved general well-being than a direct effect on muscle stem cells. However, these findings warrant further investigation.

Using a targeted fluidigm qPCR array including 48 preselected eosinophil-associated genes, we further report that eosinophils in the aging host acquire a senescent-like, pro-inflammatory phenotype (Extended Data Fig. 10 and Supplementary Table 6). This age-related eosinophil gene signature was further verified in human eosinophils (Extended Data Fig. 10c), suggesting that eosinophils might lose their migratory and regulatory function with progression of age. Consistent with the observed age-related changes in phenotype of eosinophils derived from aged donors, measures to expand endogenous eosinophils in the

aged host failed to recapitulate rejuvenating potential of transferred eosinophils from young donors (data not shown).

It has previously been reported that a sustained inflammatory milieu may promote stem cell aging[56] and contributes to the functional decline in physical and immunological performance in old age[23,43,57]. Our studies demonstrate that transfer of IL-4 competent eosinophils from young mice into aged recipients transiently restored these age-related changes in the hematopoietic stem cell pool and consequently improved physical and immunological fitness. Given the critical role of pro-inflammatory cytokines on multipotent hematopoietic progenitor cells and its effect on promoting myeloid skewing[38–41], a phenomenon commonly observed in aging, we suggest that reduction of local and systemic inflammatory mediators upon young eosinophil transfers represents an indirect mechanism to counteract these age-related hematopoietic alterations.

As the rotarod test represents a widely used paradigm to evaluate balance and motor coordination in the field of neuroscience, it is likely that transfer of IL-4 competent eosinophils from young mice into aged recipients may also improve the age-related neuromuscular decline. Consistent with this hypothesis, IL-4 treatment has been demonstrated to improve locomotor activity and reduce axon damage in experimental models of autoimmune encephalomyelitis (EAE)[58]. However, further investigations are required to analyze whether eosinophil-derived IL-4 has a direct or indirect impact on stem cell reprogramming in aged organisms.

Collectively, our studies provide strong evidence that in addition to their established role in allergic inflammation and parasite infection, eosinophils from young organisms maintain adipose tissue homeostasis and sustain physical and immunological fitness in old age. Therapeutic targeting of WAT dysfunction in aged individuals might therefore represent a new promising treatment approach to promote healthy aging.

Methods

Mouse models and drug treatment.

Wild-type (WT) C57BL/6 young (2–3 months) and aged mice (18–22months) were purchased either from Janvier Labs or Envigo and housed in specific pathogen-free (SPF) conditions at the central animal facility of the Medical School of the University of Bern. IL-5 transgenic mice (C57BL/6J-Tg(Il5)1638Jlee, kindly provided by Prof. James J. Lee and Prof. Hans-Uwe Simon), C57BL/6-Il4^{tm1Nnt} and C57BL/6-Tg(UBCGFP) 30Scha/J mice (both from The Jackson Laboratory) were bred and housed at the University of Bern and Stanford University. For transfer of IL-4 deficient eosinophils, C57BL/6J-Tg(Il5)1638Jlee mice were crossed with C57BL/6-Il4^{tm1Nnt}. For transfer of GFP+ eosinophils, C57BL/6J-Tg(Il5)1638Jlee mice were crossed with C57BL/6-Tg(UBC-GFP) 30Scha/J mice. The InVivoMAb anti-mouse IL-6 (MP5–20F3, BioXcell) was administered through intraperitoneal (i.p.) injection twice a week. Vehicle (InVivoMAb rat IgG1 Isotype control, HRPN, BioXcell) injections were performed in the same way. Treatment was initiated at 18 to 20 months of age for 4 weeks. Experiments were performed with age- and sex-matched control animals that were analyzed side by side within each experiment. Procedures

involving animal subjects have been approved by the Institutional Animal Care and Use Committee (IACUC), Stanford University and the Swiss ethical guidelines approved by the local Animal Experimentation Committee of the Canton of Bern.

Parabiosis.

Parabiosis surgery was performed as previously described[18,22]. Briefly, mice were anesthetized and the fur was shaved at adjacent flanks. Mirror-image incisions on each mouse were made through the skin. Additional incisions were made through the abdominal wall, after which the peritoneal cavities of the parabionts were sutured together. Elbow and knee joints were sutured together to facilitate ease of movement, and the skin was stapled with autoclips (Clay Adams). Parabionts were given subcutaneous injections of Baytril (antibiotic) and Buprenorphine (analgesia), and monitored during recovery, providing 0.9% saline i.p. as needed for hydration. Young isochronic mice were typically 3 months of age, heterochronics 3 and 18 months of age and old isochronics 18 months of age. After 4–5 weeks of parabiosis, pairs were sedated with i.p. chloral hydrate or tribromoethanol injections and simultaneously trans-cardially perfused with PBS before tissue collection.

Generation of BM Chimeras.

8 weeks old C57BL/6 (Ly5.1) wildtype mice were lethally irradiated by the application of 1,300 cGy as a split dose of 2 × 650 cGy with a 4 h interval, using a Gammacell 40 (GC40) research irradiator (Best Theratronics). Irradiated mice were reconstituted with 2×10^5 donor bone marrow cells from aged mice (20 months). Whole BM cells were transplanted along with congenic competitor BM cells at ratios of 1:1 to secure the survival of the chimeric mice. Antibiotics [Baytril (1.25 ml/l) and Bactrim Nopil (5 ml/l)] were supplied in the drinking water for 2 weeks. Chimerism and white blood cell populations were analyzed by flow cytometry of peripheral blood after 4, 8, 12 and 16 weeks.

Plasma collection.

Healthy human blood donors were selected by specialized academic centers based on standardized inclusion and exclusion criteria following IRB approved study protocols. Anonymized plasma samples were received together with age and gender information. Mouse blood was collected in EDTA syringes by submandibular bleeding and/or intracardial bleed at time of euthanasia. Plasma was prepared by centrifugation at 1,000g for 10 minutes at 4°C. The plasma and white blood cell fraction were recovered and prepared for subsequent flow cytometric analysis or stored at −80 °C until use.

Tissue dissection and cell preparation.

Mice were euthanized with CO_2 and trans-cardially perfused with PBS. Muscle, liver, spleen, brain, lung, kidney, thymus, skin, mesenteric lymph nodes, colon, epididymal- and subcutaneous fat were dissected, lysed, immediately snap frozen, formalin fixed or embedded in OCT for further applications. Omental adipose tissue from human donors was obtained from the University Hospital of Bern, approved by the local ethic Committee of the Canton of Bern under license 2017–01748. All donors provided informed consent. Tissue sections were immediately fixed in 4% PFA overnight and embedded in paraffin for

histological approaches. To separate adipocytes from the stromal vascular cell (SVC) fraction, visceral adipose tissue was digested in 1 mg/ml Collagenase type IV (Sigma) in RPMI medium (Gibco, supplemented with 2 nM L-glutamine, 10% FBS and 1% PenStrep) per gram tissue for 30 minutes at 37°C on an orbital shaker prior to filtration through a 70 μm cell strainer (Huber Lab). Adipocytes were separated from SVCs by centrifugation at 600g for 5 minutes. Both fractions were recovered and immediately snap frozen on dry ice or used for subsequent flow cytometric analyses after red blood cell lysis with ACK (Ammonium-Chloride-Potassium) lysing buffer.

Gene expression analysis.

For total RNA extraction 100 mg tissue was homogenized and lysed in 1 ml TRI Reagent® (Life Technologies) using a tissue lyser (Qiagen). RNA was further purified using high pure RNA kit (Roche) and quantified by measuring optical density at 280 nm wavelength (NanoDrop, Thermo Scientific). Total RNA was reverse transcribed into cDNA using Superscript III kit (Life Technologies). Real-time PCR was performed using SYBR Green technology (Applied Biosystems) with Qiagen QuantiTect qPCR primers for mouse *Actb, Tnfa, Il1b, Ccl2, Ccl11 and Il6* or human *ACTB*, *TNFA*, *IL1B*, *IL6*, *P21*, *VEGFA*. All samples were run on an Applied Biosystems 7500 Real-time PCR system. Results were normalized to the housekeeping gene *Actb* and calculated as *n*-fold induction over aged PBS control group using the ΔΔ*C*t method for all real-time PCR analyses. The fluidigm qPCR array has been performed by the Stanford Human Immune Monitoring Center. Briefly, blood eosinophils from wild-type C57BL/6 young, aged and young C57BL/6J-Tg(Il5)1638Jlee mice were sort purified directly into 1ml TRI Reagent® (Life Technologies). Total RNA was purified, reverse transcribed and used for further analysis on a fluidigm qPCR array. Results from the array were normalized to the housekeeping gene *Actb* and calculated as *n*-fold induction over young using the ΔΔ*C*t method. Values that were below detection threshold only in young samples, were imputed with a *C*t of 40 for calculation of the *n*-fold induction.

Western blotting.

Epididymal adipose tissue was prepared using M-Per lysis buffer supplemented with Halt Protease Inhibitor Cocktail (Thermo Scientific) followed by a sonication step. Total protein concentrations were determined by BCA (Pierce). Total protein (10–30 μg) was separated on a 12% SDS-polyacrylamide gel and transferred to a PVDF membrane (Biorad). Blots were blocked with 5% skim milk followed by incubation with primary antibody overnight at 4°C, washed (TBS-T) and incubated with secondary anti-mouse (Bio Rad), anti-rabbit (Bio Rad), anti-rat or anti-goat (both Santa Cruz) antibodies conjugated to horseradish peroxidase (HRP). Primary antibodies used were HSP-90α/β (0.5μg/ml), CCL2 (0.1μg/ml) and CCL11 (1μg/ml) (R&D Systems). Antibody detection reactions were developed by chemiluminescence (Pierce) and analysed using the Las3000 imaging system (Fujifilm). Band intensities at 3 different locations within each band were quantified using ImageJ software[59] and normalized to HSP-90α/β. Where indicated, levels have been calculated and expressed per total adipose tissue mass.

Enzyme-linked immunosorbent assay (ELISA).

IL-1β, IL-6, and MCP-1 cytokine levels were determined in cell lysates (from adipose tissue) and plasma samples by enzyme-linked immunosorbent assay (ELISA; IL-6 and MCP-1 from BioLegend and IL-1β from Invitrogen) using manufacturer`s instructions in 96 half-well Maxisorp plates. Cytokine binding was developed with TMB (3,3`,5,5`-tetramethylbenzidine and stopped with 1M sulphuric acid. Absorbance was measured at OD_{450} nm on a standard ELISA reader from BioTek (Bad Friedrichshall). Assay sensitivity for ELISA kits are 2pg/ml (IL-6), 30pg/ml (MCP1) and 1.2pg/ml (IL-1β).

OVA specific Serum IgG ELISA was performed as follows: ELISAs were performed with 96-half-well Maxisorp plates. Between each step, the plate was washed 4 times with 200 µl of PBS/0.05%Tween and twice with 200 µl of PBS. Ovalbumin (10ng/ml) was immobilized overnight at 4°C in 50 µl of PBS. The following day, wells were blocked with PBS/0.5% casein for 2 hours at RT. Subsequently, different mouse serum (diluted in PBS/0.5% casein) were added for 2 hours at RT. Supernatants were removed, plates were washed and further incubated with either Biotin goat anti-mouse IgG (1:1000) or biotin goat anti-mouse IgG1 (1:1000) (both BioLegend). These protein complexes were detected with poly-HRP–conjugated streptavidin (1:2500). 3,3′,5,5′-Tetramethylbenzidine was used as a substrate for HRP. The enzymatic reaction was stopped with 1 mol/l sulfuric acid, and the absorbance was measured at a wavelength of 450 nm with an EL808 plate reader (BioTek, Winooski, Vt).

Plasma of 160 human subjects between the ages of 21 and 99 years and 40 mice aged 6, 12, 18, and 24 months was measured on an antibody-based multiplex immunoassays (Luminex) by either Rules Based Medicine, a fee-for-service provider, or by the Human Immune Monitoring Center at Stanford University. All Luminex measurements where obtained in a blinded fashion. All assays were developed and validated to Clinical Laboratory Standards Institute (formerly NCCLS) guidelines based upon the principles of immunoassays as described by the manufacturers. Detection limits for individual factors are shown in Supplementary Table 3.

Flow cytometry.

Single cell suspensions were stained with live/dead stain (Life Technologies) or Propidium Iodide (BDBioscience) followed by surface staining with fluorochrome-conjugated antibodies for subsequent flow cytometric analyses. Murine cells were stained with combinations of the following antibodies: anti-mouse CD45.2 (104, BioLegend), CCR3 (J073E5, BioLegend), F4/80 (BM8, BioLegend), Siglec-F (E50–2440, BD Pharmingen, BD Bioscience), CD3e (145–2C11 and 17A2, BioLegend), CD19 (6D5, BioLegend), CD11b (M1/70, BioLegend), NK1.1 (PK136, BioLegend), VCAM (429[MVCAM.A]), integrin α7 (6A11,MBL), CD16/32 (93, BioLegend)), c-kit (2B8, BioLegend), sca-1 (D7, BioLegend), CD127 (A7R34, BioLegend), CD34 (RAM34; BioLegend), CD51 (RMV-7, BioLegend), CD31 (390, BioLegend), CD45 (30-F11, BioLegend), Ter-119 (Ter-119, BioLegend), GR-1 (RB6–8C5, BioLegend), IgD (11–26, eBioscience), B220 (RA3–6B2, BDBioscience), IgM (II-41, BDBioscience), PNA-biotin, Streptavidin-PacificBlue (Molecular Probes). CountBright™ beads (Life Technologies) were added to each sample to determine absolute cell numbers. Eosinophils were gated as live, singlet, $CD45^+$, Lin^- (CD3, CD19, NK1.1)

cells co-expressing CD11b and Siglec-F. Macrophages were gated as live, singlet, $CD45^+$, Lin^- (CD3, CD19, NK1.1) cells co-expressing CD11b and F4/80.

Human omental adipose tissue stromal vascular fraction (1×10^6 cells) was stained with live/dead stain (Life Technologies) followed by a combination of anti-human CD16 (3G8, BioLegend), Biotinylated MBP (BMK-13, BioRAD), CD11b (ICRF44, BioLegend), Siglec-8 (7C9, BioLegend), CD193 (5E8, BioLegend), CD3 (OKT3, BioLegend), CD19 (HIB19, BioLegend), CD56 (HCD56, BioLegend), Streptavidin-PE (eBioscience). Human adipose tissue eosinophils were gated as live, singlet, $CD45^+$, Lin^- (CD3, CD19, CD56), $CD16^-$, $CD11b^+$ cells co-expressing MBP and Siglec-8. Stained samples were supplemented with CountBright™ Absolute Counting Beads (Invitrogen™) and acquired on a BD LSRII flow cytometer (BD Biosciences). Data were analysed using FlowJo software (FlowJo LCC).

Sort-purification and adoptive transfers.

Terminal bleeding of wild-type, C57BL/6J-Tg(Il5)1638Jlee, C57BL/6J-Tg(Il5)1638Jlee-UBI-GFP^+ mice or C57BL/6J-Tg(Il5)1638Jlee on an IL-4 deficient background (2–3 months) was performed and red blood cells were lysed with ACK buffer. Primary eosinophils and *ex vivo* generated wild-type BMDEOS were sort purified using a BD FACSAria™ III cell sorter (BD Bioscience) to ≥ 98% purity as live, $CD45^+$, $CD3^-$, $CD19^-$, $NK1.1^-$, $GR1^{Int}$, $CD11b^+$, Siglec-F^+ cells. 1.5×10^6 eosinophils were immediately transferred via intraperitoneal (i.p.) injection to indicated aged recipients. Transfers were performed twice a week for 4 consecutive weeks. In some studies, mice were treated with eosinophils for once, 2 times a week or for 5 weeks, twice a week. As a control group, live, $CD45^+$, $CD3^-$, $CD19^-$, $NK1.1^-$, $Ly6G^+$, $CD11b^+$ neutrophils were isolated from the bone marrow of WT C57BL/6 mice (2–3 months) and 1.5×10^6 cells were injected i.p. into aged mice twice a week for 4 consecutive weeks. When indicated, eosinophils were pre-treated in vitro with 100 ng/ml pertussis toxin (Sigma-Aldrich) for 2 h at 37°C in complete RPMI 1640 Medium and/or sort-purified eosinophils were labelled with CSFE (Molecular probes) using standard protocols to distinguish endogenous from transferred eosinophils.

Isolation of muscle stem cells.

Muscle stem cells (satellite cells) were isolated as described previously[60]. In brief, muscle tissues from hind limb were collected and minced for 10 min in 50 ml Falcon tubes in 5 ml RPMI. 5 ml collagenase (Sigma, 1mg/ml) were added and incubated on a shaker for 1 hour at 37° at 70 rpm (horizontal). Cells were washed with RPMI and centrifuged for 5 minutes at 500 g at 4 °C. Supernatant was aspirated down to 8 ml and 1 ml (collagenase 10 mg/ml) and 1ml (Dispase, Roche, 10 mg/ml) in PBS. Suspension was carefully triturated 10–15 times up and down using a 20 ml pipette without clogging. Samples were incubated for 30 minutes on an orbital shaker. A 35 ml syringe with a 21-gauge needle was used to aspirate and eject the muscle suspension in and out of the syringe 10 times. Cell suspension was washed in RPMI and cells were transferred to a 70 μm nylon cell strainer and washed again at 500 g for 5minutes at 4 °C. Satellite cells were sort-purified as $CD45^-$, $CD31^-$, $Sca\text{-}1^-$ cells co-expressing $Vcam^+$ and $Integrina7^+$.

Histological and immunohistochemistry analysis.

Omental adipose tissue from human donors, perfused mouse visceral adipose tissue and perfused hindlimb muscles were PFA fixed overnight and embedded in Paraffin. Tissue sections (8 μM) were either stained with H&E or processed for immunofluorescence staining.

Adipocyte size and numbers were assessed in H&E stained slides. Digital images were captured at ×10 magnification using Pannoramic caseViewer (3DHISTECH LTD.). Computerized morphometric analysis (ImageJ software) of individual adipocyte sections was performed in a blinded fashion. Approximately 500–1000 adipocytes per sample were measured. Eosinophils in human omental adipose tissue sections were enumerated in H&E stained slides. Digital images were analysed at ×30 magnification using Pannoramic caseViewer (3DHISTECH LTD.). Eosinophils were defined by nuclear morphology (nucleus with 2 lobes) und cytoplasmic pink color. Blinded and randomized $1cm^2$ sections were independently quantified by 2 researchers. Centrally nucleated myofibers were enumerated in randomized and blinded H&E stained longitudinal and cross-sectional mouse muscle sections.

For cellular immunostaining, samples were first dewaxed (Xylol/EtOH) followed by antigen retrieval with Pepsin reagent for 20 minutes at 37°C. Samples were washed 3 times in TBS-0.1%Triton (TBS-T) and blocked in TBS-T BSA for 1 h room temperature in a humidified chamber. Primary antibodies were applied overnight at 4 °C in TBS-T-BSA (anti-human MBP; 1:20, BioRAD, anti-mouse MBP; 1:250 (provided by Dr Jamie Lee), anti-mouse Perilipin; 1:200; Novus Biological). Sections were stained with secondary antibody (goat anti-mouse IgG Alexa Flour 568, goat anti-rabbit IgG Alexa Fluor 488 or goat anti-rat IgG Alexa Fluor 568, Invitrogen) for 1 h at room temperature and mounted with Prolong Diamond Antifade Mountant with DAPI (Invitrogen) before imaging on a 3D Histech slide scanner Pannoramic 250 Flash II (3DHISTECH LTD.) or on a Zeiss Axio Imager.A2 microscope (Zeiss).

Cultured MuSCs (formed myotubes) were fixed at day 7 in 4 % PFA and stained with HSP90 (H-114, Santa Cruz) followed by goat anti-rabbit Alexa 488 (Invitrogen) for visualization. Slides were mounted with Prolong Diamond Antifade Mountant with DAPI (Invitrogen) before imaging and pictures were taken on an Axio Imager A2 (Zeiss). Area and number of differentiated satellite cells were quantified using ImageJ. 5. one random area from each tissue section were used for quantification.

Bone marrow derived eosinophil (BMDEos) cultures.

Eosinophils were generated from bone marrow as described previously[61]. In brief, bones of wild-type mice were flushed from femur and tibia. Red blood cells were removed from single cell suspension by hypotonic lysis. Bone marrow cells were cultivated in bone marrow medium (BMMC-Medium, RPMI-1640, GIBCO) 20% FBS, 10 U/ml penicillin, 10 μg/ml streptomycin, 2 mM glutamine, 25 mM HEPES, 1 x nonessential amino acids, 1mM sodium pyruvate, 50 μM 2-ME (all from Life Technologies). Cells were cultured with 100 ng/ml of stem cell factor (SCF) and 100 ng/ml of fms-like tyrosine kinase 3 ligand (FLT3L,

both PeproTech) for 4 days. At day 4, medium was exchanged and supplemented with 10 ng/ml of recombinant murine IL-5 (R&D Systems). Half of the medium was replaced every other day from day 8 on. BMDEos were sort-purified at day 14.

Myogenesis assay.

1500 Muscle stem cells (satellite cells) were sorted-purified and plated into wells of a Matrigel (Corning)-coated 24- well cell culture plate, containing MuSC growth medium (Ham's F-10 Nutrient Mix; Thermo Fisher scientific), 20% FBS, 1x Pen/Strep and 2.5 ng/ml hBFGF (Sigma) as previously reported[62]. Cells were cultured at 37 °C for 7 days. Growth factor was added daily (2.5 ng/ml). Myotubes were stained and quantified as described in histological analysis section.

Isolation of primary human eosinophils.

Human eosinophils were isolated from volunteers who provided informed consent in accordance with the Declaration of Helsinki. The study has been approved by the local ethic Committee under license 108/14. Donors were defined by age (young ≤ 29 and old ≥ 64). In brief, peripheral human blood granulocytes were purified from venous EDTA-blood by dextran sedimentation of red blood cells followed by Percoll density gradient centrifugation (1.0791 and 1.0695 and 1.901 g/ml, GE Healthcare) and further purified by negative selection (anti-CD16 Microbeads and Glycophorine A beads, Miltenyi Biotec). Eosinophils were gated as $CD16^{-}$, $CD193^{+}$ and $Siglec\text{-}8^{+}$ cells and absolute cell numbers and purity (≥ 90%) were assessed by a FACSCalibur flow cytometer (Becton Dickinson) using BD Truecount Tubes (BD Biosciences).

Physical function measurements.

A grip strength meter (Bioseb, France) was used to assess the limb strength of aged mice. To determine maximal peak force each mouse was pulled backwards parallel to the metal bar after allowing the mice to grab with their forelimbs. Grip strength was measured 3 times with 5 minutes intervals between triplicate measurements. Mice were adapted to the grip strength test the day before analysis. To measure forced physical activity, animals were assessed for their ability to stay on a 7 cm diameter Rotarod (Ugo Basile, Italy). Mice were placed on the drum rotating at constant speed of 4 rpm for 20 seconds following constant acceleration. Mice were adapted to the Rotarod device before they performed 4 test runs. The speed was recorded when the mouse dropped off the Rotarod. Results were averaged from 4 trials and normalized, where indicated, to the baseline speed at T zero. Data are displayed as average of the test runs. Baseline measurements for grip strength and Rotarod were taken at T_{zero}. Differences between T_{final} (4 Test runs) and T_{zero} (2–3 Test runs) for Rotarod and differences between T_{final} and T_{zero} (for both, average of 9 Test runs) for grip strength were calculated for each individual mouse to determine the rejuvenating potential. Open field tests were used to assay general voluntary locomotor activity. In brief, mice were placed in an enclosed, rectangular box (35 cm × 54 cm) and movements in a dedicated arena were tracked for 10 minutes using the EthoVision™ system (Noldus). Movement velocity, total distance moved, accumulative mobility and immobility were recorded.

Stem cell analysis.

BM lineage depletion was performed using biotinylated antibodies against red cell precursors (αTer119), B cells (αCD19), T cells (αCD3ε) and myeloid cells (αGr1), MACS αbiotin beads and LS columns (Miltenyi Biotec). Colony formation assays were performed as previously described[40]. Briefly, 3.3×10^3 Lin^- cells were cultured in MethoCult base medium (STEMCELL Technologies) supplemented with 15% FCS, 20% BIT (50 mg/ml BSA in Iscove's modified Dulbecco's medium, 1.44 U/ml rh-insulin [Actrapid, Novo Nordisk], and 250 ng/ml human Holo Transferrin [ProSpec]), 100 μM 2-β-mercaptoethanol, 100 U/ml penicillin, 100 μg/ml streptomycin, 2 mM L-glutamine, and a cytokine mix of 50 ng/ml rm-SCF, 10 ng/ml rm-IL-3, 10 ng/ml rh-IL-6, and 50 ng/ml rm-Flt3-ligand (all from ProSpec). Total colonies and colony subsets were enumerated after 7 days.

Mesenchymal stem cells (MSCs) were analysed by flow cytometry as previously described[40]. Briefly, bones were crushed and digested in PBS with collagenase and DNase for 1 h at 37°C. Stromal cells were separated from the hematopoietic fraction by removing $CD45^+Ter\text{-}119^+$ cells by MACS. Cells were stained for CD51, Sca-1, and CD31. Hematopoietic cells were excluded with lineage markers, CD45, and Ter-119.

Immunization.

Mice were immunized with Ovalbumin (OVA) emulsified in complete Freund`s adjuvant (OVA-CFA) according to the manufacturers protocol (Hooke Laboratories). In brief, anesthetized mice were immunized with 100 μl OVA-CFA subcutaneously at two sites on the back. Fourteen days later mice received a secondary subcutaneous injection (100 μl) with OVA emulsified in incomplete Freund's adjuvant (OVA-IFA). Seven days after secondary immunization the spleens were harvested and analyzed.

ELISpot.

Single cell splenocyte suspensions were prepared by squeezing dissected spleens through a 70 μm cell strainer. Red blood cells were lysed using ACK buffer and samples centrifuged. Supernatants were discarded and cells resuspended in RPMI medium. Cells were counted using a Neubauer chamber and diluted to 2.5×10^6 cells/ml. Three 1:4 serial dilutions of cells were prepared. ELISpot plates (Milipore) were coated overnight at 4°C with 15 μg/ml ovalbumin (Sigma) in carbonate buffer (pH 9.6). Plates were washed two times with PBS and each well blocked with 4% skim milk for 2 hours at 37°C. Subsequently, plates were washed with PBS. 100 μL of serially diluted cells were added to the wells and incubated for 12 hours at 37°C/ 5% CO_2. Subsequently, cells were discarded and wells washed with PBS/ 0.05% Tween and PBS. Goat-anti-mouse IgG (AT-2306–2, EY Laboratories) was added at a 1:1000 dilution in blocking buffer for 9 hours at room temperature. Wells were washed with PBS/ 0.05% Tween and PBS. Donkey anti-goat alkaline phosphatase (705-055-147, Jackson Immunochemicals) was added at 1:1000 in blocking buffer and incubated for 3 hours at room temperature on a shaker. Wells were washed with PBS/ 0.05% Tween and PBS. 50 μL development solution AP Conjugate Substrate Kit (1706432, BioRad) were added to each well for 3 minutes and the reaction was stopped with deionized water. Immunospots were quantified using an ELISpot reader (AID GmbH).

Proteomic analysis of plasma samples.

Proteomic analysis was performed in Prism (GraphPad Software) and the open source software R[63]. The human and mouse plasma datasets were pre-processed as follows: factors with more than 85% missing values due to concentrations below the detection threshold were excluded. For the remaining factors missing values were imputed with the lowest measurable concentration. The plasma data was standardized by log2 transformation and z-scoring[64]. Outliers defined as subjects with more than one factor that is more than 3 standard deviations away from the mean were excluded from the dataset. In order to get maximal matching of age and gender distribution 10 male and 10 female subjects were randomly selected per age group from the human dataset. In the mouse cohort 5 males and 5 females were included per age group. The open source software Gene Cluster 3.0[65] was used for unsupervised clustering of mean values from each age group. Data was visualized using the open source software Java TreeView[66]. R software was used to calculate Spearman's rank correlations between measured factors and age.

Data and statistical analysis.

All data are expressed as mean ± standard error of the mean (S.E.M.) unless stated otherwise. All experiments were conducted in a randomized and blinded fashion. All treatment groups were compared for statistical analysis using GraphPad Prism 7.0 (GraphPad Software, Inc.). Pearson correlation, unpaired two-tailed Student's *t*-tests, paired *t*-tests were used to estimate statistically significant differences between two groups or repeated measurements within one group, respectively. One-way analysis of variance (ANOVA) followed by two-tailed post-hoc Dunnett's multiple comparison test was used for multiple comparison. Significance was set at $p < 0.05$.

Data availability.

Additional data that support the findings of this study are available from the corresponding authors upon reasonable request. Source data for Extended Data Fig. 1 are available online.

Supplementary Material

Refer to Web version on PubMed Central for supplementary material.

Extended Data

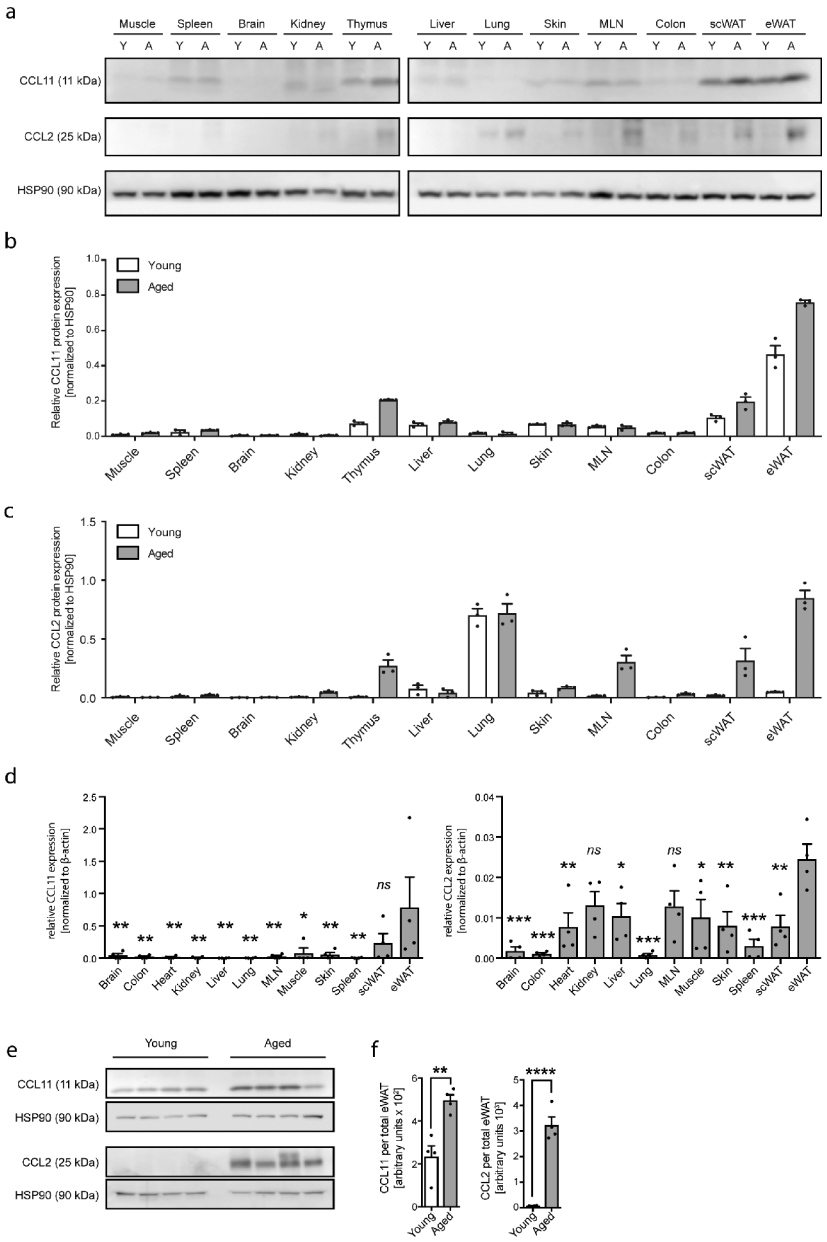

Extended Data Fig. 1. Tissue screens for CCL11 and CCL2 protein expression in young and aged mice.

(a) Comparison of CCL11 and CCL2 protein expression in muscle, spleen, brain, kidney, thymus, liver, lung, skin, mesenteric lymph nodes (MLN), colon, subcutaneous WAT (scWAT) and epididymal WAT (eWAT) of young (Y, 2–3 months) and aged mice (A, 18–20 months) as assessed by western blot. Tissues of three biologically independent animals were pooled. HSP90 served as loading control. Quantification of (b) CCL11 and (c) CCL2 protein levels normalized to HSP90 in indicated tissues of young (Y, 2–3 months) and aged mice (A, 18–20 months) by ImageJ. One out of two independently performed experiments is shown. (d) Comparison of CCL11 and CCL2 mRNA expression levels in indicated tissues of aged mice (18–20 months) as assessed by qPCR (n=4). (e) CCL2 and CCL11 protein levels were assessed by western blot (n=4). One out of 3 independently performed experiments is

shown. (f) Quantification of CCL11 and CCL2 protein levels normalized to HSP90 in indicated tissues of young (Y, 2–3 months, n=4) and aged mice (A, 18–20 months, n=4). HSP90 served as loading control. Protein levels from total eWAT was calculated. Statistical significance was calculated by one-way ANOVA followed by two-tailed post-hoc Dunnett's multiple comparison test against eWAT (d) or by unpaired two-tailed Student's t test between young and aged samples (f). Data are shown as individual data points with mean ± SEM. *p < 0.05, **p < 0.01, ***p < 0.001. Uncropped western blots are provided in the Source Data File.

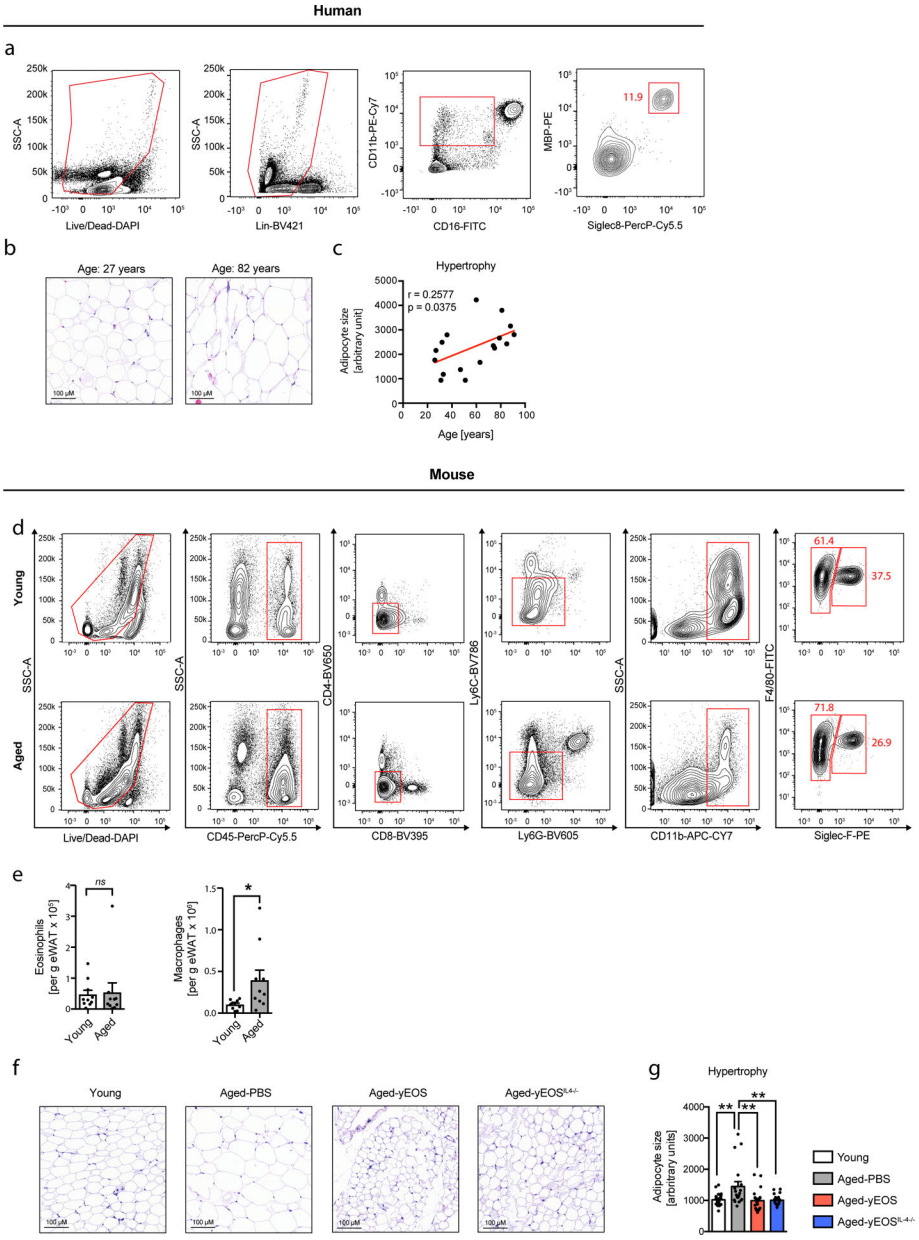

Extended Data Fig. 2. Gating strategies for human and mouse ATEs and age-related adipose tissue hypertrophy.

(a) Experimental protocol. (b) Frequencies of eosinophils, macrophages and calculated eosinophil:macrophage ratios in eWAT of Aged-PBS (n=8) and Aged-yNEU (n=9) mice. (c) mRNA expression levels for *Tnfa, Il1β* and *IL6* in eWAT of Aged-PBS (n=8) and Aged-yNEU mice (n=9). Data are presented as fold induction over Aged-PBS controls. (d) Average time on Rotarod of Aged-PBS controls (n=8) and Aged-yNEU mice (n=9). (e) Total numbers of lin$^-$, Sca-1$^+$, c-kit$^+$ hematopoietic stem cells (LSKs) in Aged-PBS (n=4) and Aged-yNEU (n=4) mice. (f) Numbers of common myeloid progenitors (CMP), common lymphoid progenitors (CLP), and granulocyte/monocyte progenitors (GMP) in the bone marrow of Aged-PBS (n=4) and Aged-yNEU (n=4) mice. (g) Frequencies of neutrophils in eWAT of young (n=5), Aged-PBS (n=4) and Aged-yNeu (n=5) mice. (h) Experimental

protocol of bone marrow derived eosinophil (BMDE) transfers. (i) Calculated ATE:ATM ratios in eWAT of Aged-PBS (n=5) and Aged-BMDE (n=4) mice as measured by flow cytometry. (j) IL-6 protein levels in eWAT of Aged-PBS (n=6) and Aged-BMDE (n=5) mice. (k) Pre- and post-treatment IL-6 plasma protein levels in Aged-PBS (n=6) and Aged-BMDE (n=5). (l) Intra-group and (m) inter-group comparison of pre- and post-treatment average time on wheel (Rotarod test) in Aged-PBS (n=6) and Aged-BMDE (n=5) mice. Delta in performances in (l) is calculated relative to baseline (post- minus pre-treatment results). Statistical significance was calculated by Wilcoxon matched pairs signed rank test (k, l), by unpaired two-tailed Student's t test (b, c, d, e, f, I, j, m) or by one-way ANOVA followed by two-tailed post-hoc Dunnett's multiple comparison test against the aged-PBS treated group (g). Data are pooled from two independently performed experiments (except for (g-m) only one experiment has been performed) and shown as individual data points with mean ± SEM. Data are shown as mean ± SEM. *$p < 0.05$, **$p < 0.01$.

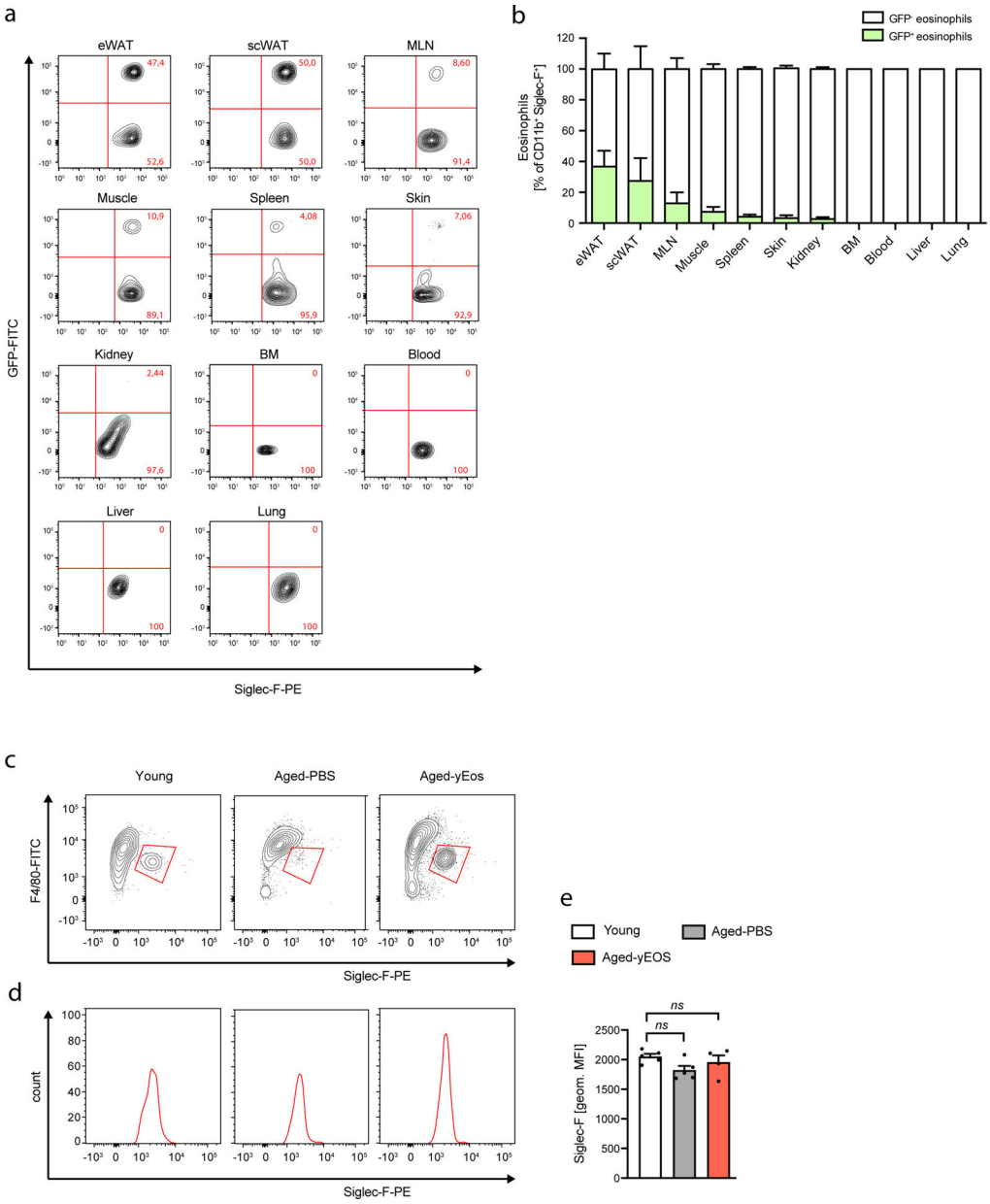

Extended Data Fig. 3. Recruitment of sort-purified GFP+ eosinophils to WAT of aged mice.

Aged mice (18 months) were adoptively transferred with sort-purified GFP^+ eosinophils derived from IL-5 transgenic mice on two subsequent days. The following day eosinophil recruitment into different tissues was assessed by flow cytometry. (a) Representative flow plots of transferred GFP^+ and endogenous GFP^- tissue eosinophils in indicated tissues. (b) Frequencies of transferred GFP^+ and endogenous GFP^- tissue eosinophils in indicated tissues. (c) Siglec-F surface expression on adipose tissue eosinophils from Young, Aged-PBS and Aged-yEOS -treated mice as assessed by flow cytometry. (d) Representative histograms of Siclec-F expression on ATEs of indicated groups. (e) Quantification of Siglec-F surface expression (MFI) on adipose tissue eosinophils of Young (n=5), Aged-PBS (n=5) and Aged-yEOS (n=4) mice. The experiment was done once. Statistical significance was

calculated by one-way ANOVA followed by two-tailed post-hoc Dunnett's multiple comparison test against the young group. *ns* = not significant. Data are representative of $n=4$ per group and are shown as mean ± SEM.

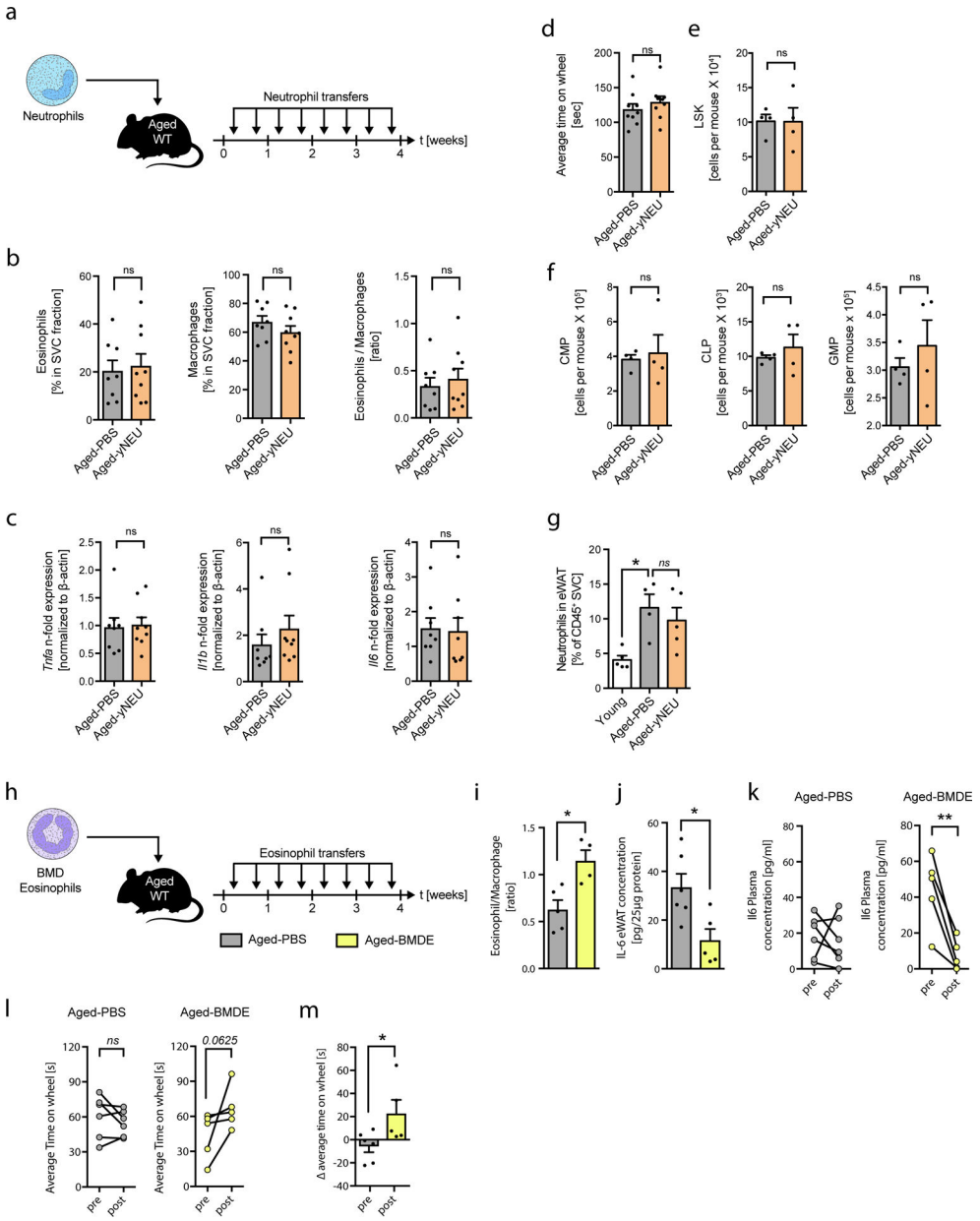

Extended Data Fig. 4. Transfer of neutrophils to aged mice does not alter WAT inflammation, hematopoetic stem cell pol or physical performance.

(a) Experimental protocol. (b) Frequencies of eosinophils, macrophages and calculated eosinophil:macrophage ratios in eWAT of Aged-PBS (n=8) and Aged-yNEU (n=9) mice. (c) mRNA expression levels for *Tnfa, Il1β* and *IL6* in eWAT of Aged-PBS (n=8) and Aged-yNEU mice (n=9). Data are presented as fold induction over Aged-PBS controls. (d) Average time on Rotarod of Aged-PBS controls (n=8) and Aged-yNEU mice (n=9). (e) Total numbers of lin$^-$, Sca-1$^+$, c-kit$^+$ hematopoietic stem cells (LSKs) in Aged-PBS (n=4) and Aged-yNEU (n=4) mice. (f) Numbers of common myeloid progenitors (CMP), common lymphoid progenitors (CLP), and granulocyte/monocyte progenitors (GMP) in the bone marrow of Aged-PBS (n=4) and Aged-yNEU (n=4) mice. (g) Frequencies of neutrophils in eWAT of young (n=5), Aged-PBS (n=4) and Aged-yNeu (n=5) mice. (h) Experimental

protocol of bone marrow derived eosinophil (BMDE) transfers. (i) Calculated ATE:ATM ratios in eWAT of Aged-PBS (n=5) and Aged-BMDE (n=4) mice as measured by flow cytometry. (j) IL-6 protein levels in eWAT of Aged-PBS (n=6) and Aged-BMDE (n=5) mice. (k) Pre- and post-treatment IL-6 plasma protein levels in Aged-PBS (n=6) and Aged-BMDE (n=5). (l) Intra-group and (m) inter-group comparison of pre- and post-treatment average time on wheel (Rotarod test) in Aged-PBS (n=6) and Aged-BMDE (n=5) mice. Delta in performances in (l) is calculated relative to baseline (post- minus pre-treatment results). Statistical significance was calculated by Wilcoxon matched pairs signed rank test (k, l), by unpaired two-tailed Student's t test (b, c, d, e, f, I, j, m) or by one-way ANOVA followed by two-tailed post-hoc Dunnett's multiple comparison test against the aged-PBS treated group (g). Data are pooled from two independently performed experiments (except for (g-m) only one experiment has been performed) and shown as individual data points with mean ± SEM. Data are shown as mean ± SEM. *$p < 0.05$, **$p < 0.01$.

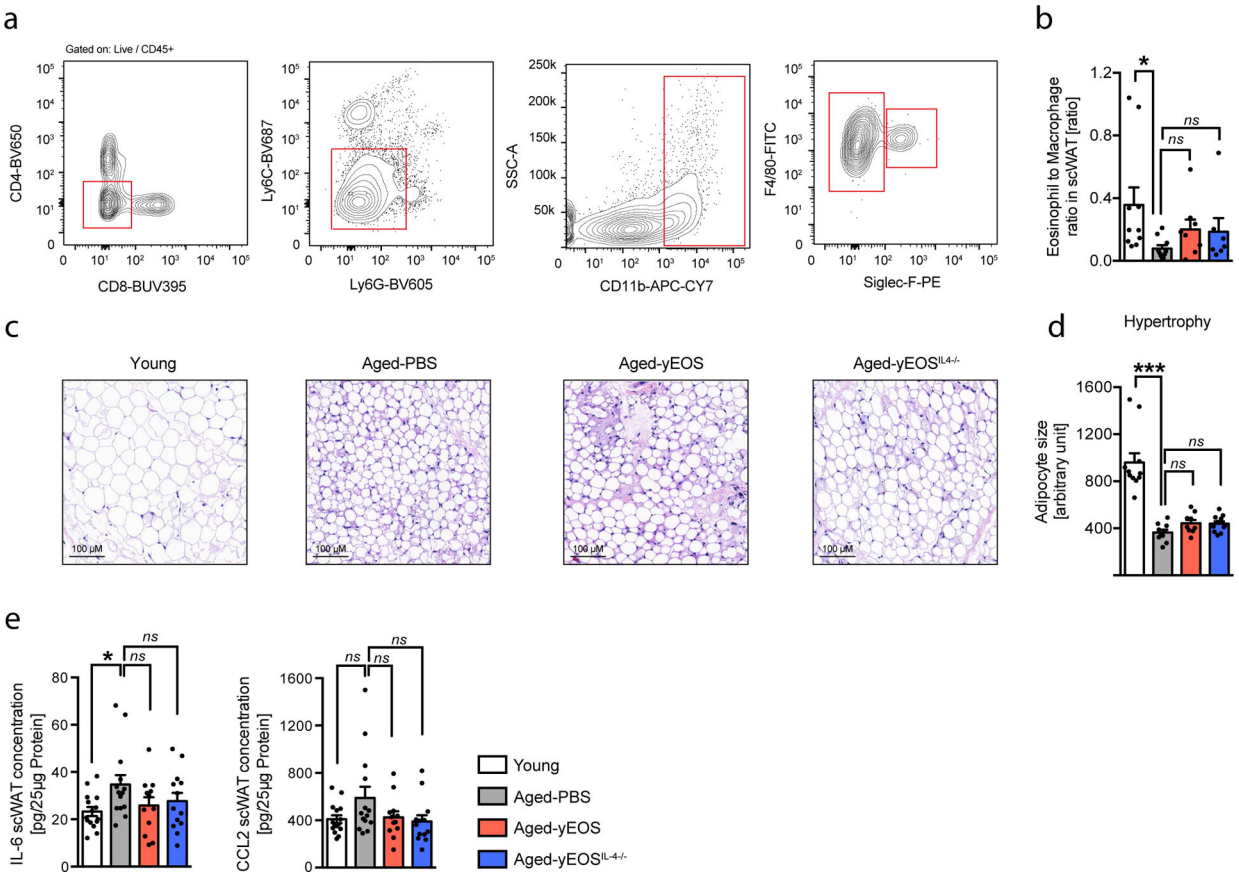

Extended Data Fig. 5. Eosinophil transfers do not alter age-related changes in murine subcutaneous WAT.

(a) Gating strategy for ATMs and ATEs in scWAT of young (3 months) and aged (20 months) mice. (b) Calculated ATE:ATM ratio in scWAT of young (n=10), Aged-PBS (n=10), Aged-yEOS (n=6) and Aged-yEOS$^{IL-4-/-}$ (n=7) mice. (c) Representative photographs of H&E stained histological scWAT sections of indicated treatment groups. (d) Quantification of adipocyte hypertrophy in Young (n=11), Aged-PBS (n=10), Aged-yEOS (n=9) and Aged-yEOS$^{IL-4-/-}$ (n=12) mice by ImageJ. (e) IL-6 and CCL2 protein levels in scWAT of Young (n=15), Aged-PBS (n=14), Aged-yEOS (n=12) and Aged-yEOS$^{IL-4-/-}$ (n=13) mice. Statistical significance was calculated by one-way ANOVA followed by two-tailed post-hoc Dunnett's multiple comparison test against the aged-PBS treated group. Data (e) are pooled from 2 independently performed experiments or performed once (a-d) and shown as individual data points with mean bars ± SEM. *p < 0.05, **p < 0.01, ***p < 0.001.

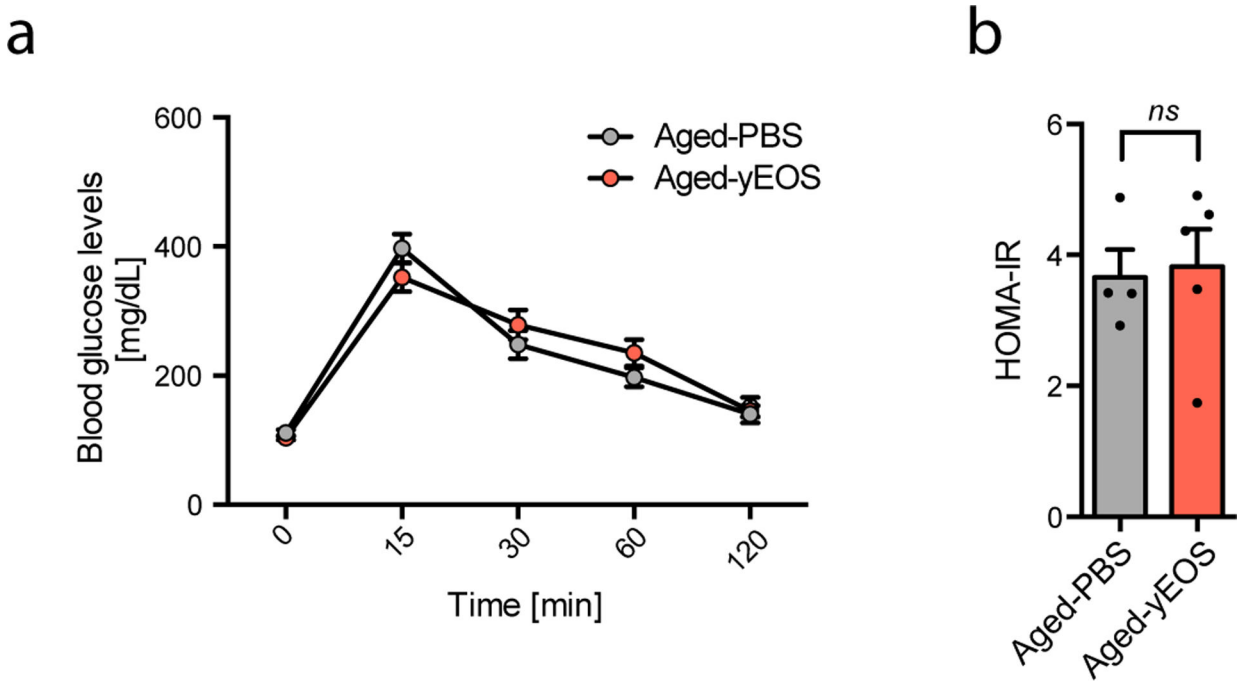

Extended Data Fig. 6. Surface expression of Siglec-F on WAT resident and transferred eosinophils and glucose metabolism in response to eosinophil transfers to aged mice.

(a) Blood glucose levels in Aged-PBS (20 months, *n*=4) and Aged-yEOS (*n*=5) mice in response to i.p. glucose challenge over time. (b) Calculated HOMA-IR for Aged-PBS (20 months, *n*=4) and Aged-yEOS (20 months, *n*=5) mice. Statistical significance was tested by unpaired two-tailed Student's *t*-test. One out of 3 independently performed experiments is shown. Data are shown as individual data points with mean bars ± SEM. **p < 0.01.

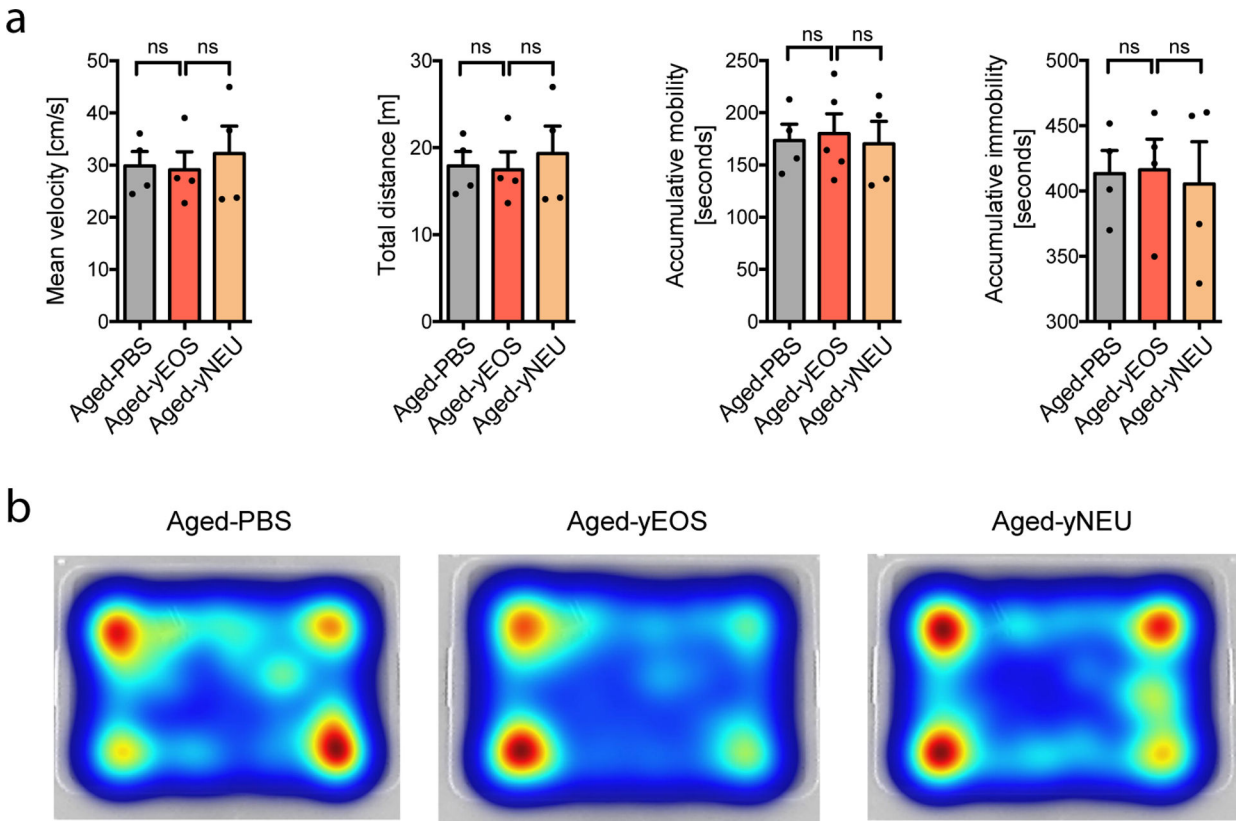

Extended Data Fig. 7. Open field activity tests.

(a) Mean velocity, total distance, accumulative mobility- and immobility of Aged-PBS, Aged-yEOS and Aged-yNEU mice (n=4 per group). (b) Representative heat maps for Aged-PBS, Aged-yEOS and Aged-yNEU mice demonstrating the animal's position in the arena. The experiment was done once. Statistical significance was calculated by one-way ANOVA followed by two-tailed post-hoc Dunnett's multiple comparison test against the aged-PBS treated group. Data are shown as mean bars ± SEM. ns: not significant.

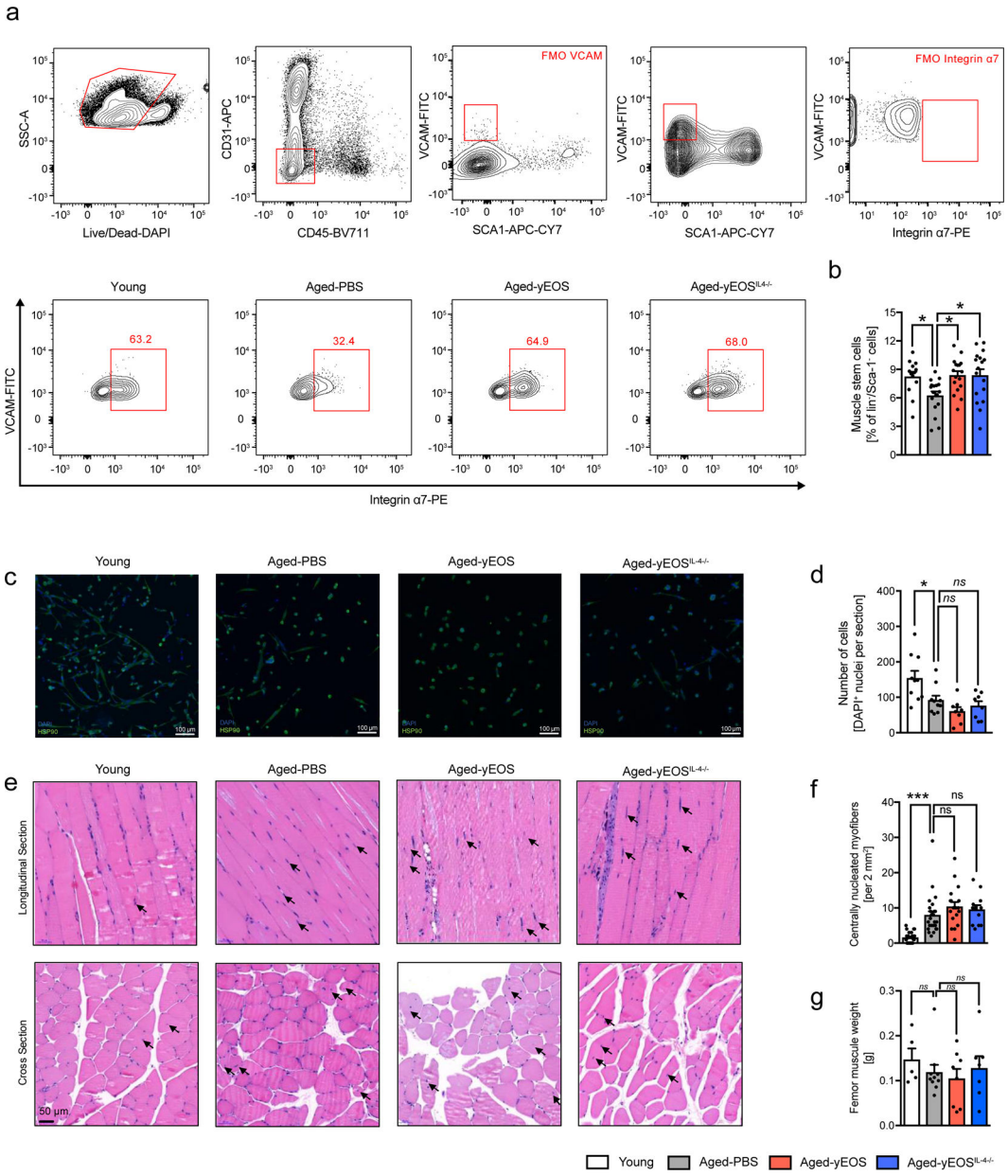

Extended Data Fig. 8. Transfer of young eosinophils is associated with alterations in muscle stem cell frequencies but not function.

(a) Gating strategy and representative flow plots of CD31^{-}, CD45^{-}, Sca-1^{-}, Vcam^{+} and integrin α7^{+} satellite cells in muscle of Young (n=13), Aged-PBS (n=17), Aged-yEOS, (n=17) and Aged-yEOS$^{IL-4-/-}$ (n=17) mice. (b) Quantification of muscle stem cell frequencies in indicated groups (c) Representative photographs of immunofluorescent stained sort-purified and differentiated satellite cells. (d) Quantification of cell colony formation of sort-purified muscle stem cells of Young (n=10), Aged-PBS (n=10), Aged-yEOS (n=8) and Aged-yEOS$^{IL-4-/-}$ (n=8) mice (e) Representative H&E stained longitudinal and cross-sectional quadriceps femoris in indicated groups. (f) Quantification of centrally nucleated myofibers in sections of Young (n=26), Aged-PBS (n=26), Aged-yEOS (n=18) and Aged-yEOS$^{IL-4-/-}$ (n=13) mice. (g) Muscle weight (femur) was measured in Young

(*n*=5), Aged-PBS (*n*=9), Aged-yEOS (*n*=8) and Aged-yEOS$^{IL-4-/-}$ (*n*=7) mice. Data (a-f) are pooled from 2 independently performed experiments except for g (one experiment has been performed). Statistical significance was calculated by one-way ANOVA followed by two-tailed post-hoc Dunnett's multiple comparison test against the aged-PBS treated group. Data are shown as individual data points with mean ± SEM. *p < 0.05, **p < 0.01, ***p < 0.001.

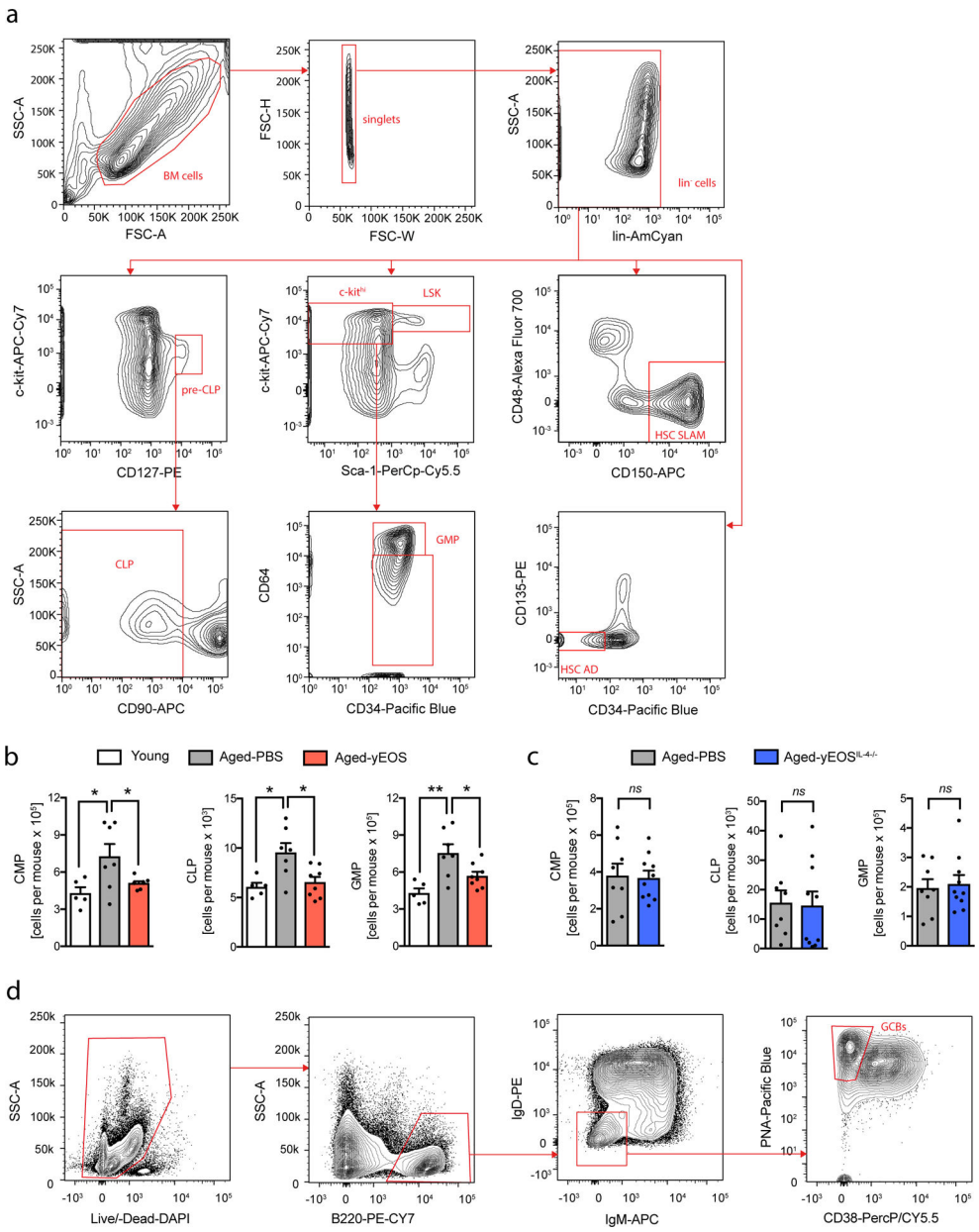

Extended Data Fig. 9. Eosinophil transfers reverse myeloid skewing in old age.

(a) Gating strategy for the identification of LSK, HSC-SLAM, HSC-AD, CMP, CLP and GMP populations. (b) Absolute numbers of CMP, CLP and GMP per mouse in Young (*n*=5), Aged-PBS (*n*=7) and Aged-yEOS (*n*=8) groups. (c) Absolute numbers of CMP, CLP and GMP per mouse in Aged-PBS (*n*=8) and Aged-yEOS$^{IL-4-/-}$ (*n*=10) groups. One out of two independently performed experiments is shown and data are shown as individual data points with mean ± SEM. Statistical significance in (b) was calculated one-way ANOVA followed by two-tailed post-hoc Dunnett's multiple comparison test against the aged-PBS treated group and (c) by two-tailed Student's *t*-test. (d) Gating strategy for the identification of germinal GCB. Data are shown as individual data points with mean ± SEM. *p < 0.05, **p < 0.01, ***p < 0.001.

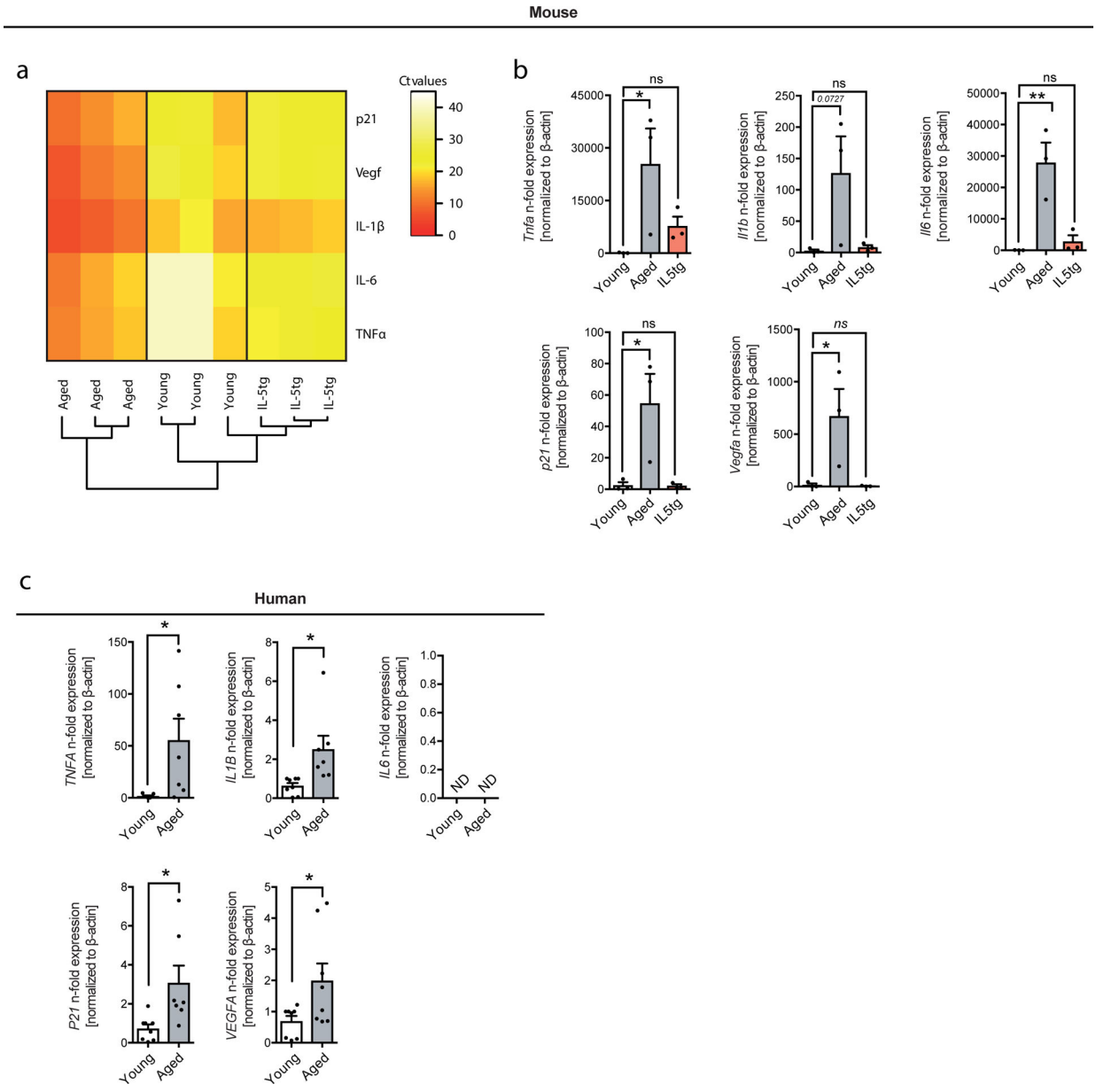

Extended Data Fig. 10. Eosinophils adopt a senescent-like inflammatory phenotype with age.

(a) Heat map representing *Ct* values of *p21, Vegfa, Il1b, Il6* and *Tnfa* in sort-purified, blood-derived eosinophils from aged WT (20 months), young WT (3 months) or young IL5 transgenic mice (3 months) as assessed by targeted fluidigm qPCR array. (b) Relative expression levels of *Tnfa, Il1b, Il6, p21* and *Vegfa* in sort-purified, blood-derived eosinophils from aged WT (20 months), young WT (3 months) or young IL5 transgenic mice (3 months) as assessed by fluidigm qPCR array. Eosinophils from 3 animals were pooled for each measurement (n=3 per group). The experiment was done once. (c) Relative expression levels of *TNFa, IL1b, IL6, p21* and *VEGFA* in human blood derived eosinophils from young (average age=34, *n*=8) and aged (average age=64, *n*=7) donors. Data in (b and c) are shown as individual data points with mean ± SEM and statistical significance was calculated by one-way ANOVA followed by two-tailed post-hoc Dunnett's multiple comparison test

against the young group (b) and two-tailed students *t*-test (c). *$p < 0.05$, **$p < 0.01$, ***$p < 0.001$. ND: not detectable.

Acknowledgments:

We thank past and present members of the Noti, Eggel and Wyss-Coray labs for discussions and valuable input; Anne-Laure Huguenin, Ursina Lüthi and Caroline Krüger for technical support; Prof. James J. Lee and Prof. Hans-Uwe Simon for providing IL-5 transgenic mice; Dr. Michaela Fux, Andrea Odermatt, and the DBMR FACSlab for technical support concerning cell sorting; the staff and animal caretakers of the Central Animal Facility in Bern for their advice and support; Dr. Kaspar Rufibach for valuable discussions; Prof. Holden Maeker and the Stanford Human Immune Monitoring Center for their help with the qPCR multiplex array. J.A. is supported by grants from the École Polytechnique Fédérale de Lausanne, the Swiss National Science Foundation (31003A-140780), the AgingX program of the Swiss Initiative for Systems Biology (51RTP0-151019), and the NIH (R01AG043930). Further, this work was funded by the National Institute on Aging (R01AG053382 to S.A.V., AG045034 and OD020772 to T.W.C.), the Department of Veterans Affairs (to T.W.C.), the Glenn Center for the Biology of Aging (to T.W.C.), a Novartis grant for Medical-Biological Research (15B100 to M.N.), a FreeNovation Novartis grant (to M.N), grants from the Fondation Acteria (to A.E. and M.N.) and a grant from the Velux Stiftung (1095 to. A.E.). The authors have no conflicts of interest.

References:

1. Palmer AK & Kirkland JL Aging and adipose tissue: potential interventions for diabetes and regenerative medicine. Exp Gerontol 86, 97–105 (2016). [PubMed: 26924669]
2. Barzilai N, Banerjee S, Hawkins M, Chen W & Rossetti L Caloric restriction reverses hepatic insulin resistance in aging rats by decreasing visceral fat. J Clin Invest 101, 1353–1361 (1998). [PubMed: 9525977]
3. Finkel T The metabolic regulation of aging. Nat Med 21, 1416–1423 (2015). [PubMed: 26646498]
4. López-Otín C, Galluzzi L, Freije JMP, Madeo F & Kroemer G Metabolic Control of Longevity. Cell 166, 802–821 (2016). [PubMed: 27518560]
5. Gabriely I et al. Removal of visceral fat prevents insulin resistance and glucose intolerance of aging: an adipokine-mediated process? Diabetes 51, 2951–2958 (2002). [PubMed: 12351432]
6. Muzumdar R et al. Visceral adipose tissue modulates mammalian longevity. Aging Cell 7, 438–440 (2008). [PubMed: 18363902]
7. Fontana L, Partridge L & Longo VD Extending healthy life span--from yeast to humans. Science 328, 321–326 (2010). [PubMed: 20395504]
8. Colman RJ et al. Caloric restriction delays disease onset and mortality in rhesus monkeys. Science 325, 201–204 (2009). [PubMed: 19590001]
9. Mattison JA et al. Caloric restriction improves health and survival of rhesus monkeys. Nat Commun 8, 14063 (2017). [PubMed: 28094793]
10. Weindruch R The retardation of aging by caloric restriction: studies in rodents and primates. Toxicol Pathol 24, 742–745 (1996). [PubMed: 8994305]
11. Xu M et al. Senolytics improve physical function and increase lifespan in old age. Nat Med 55, 1–1256 (2018).
12. Hahn O et al. A nutritional memory effect counteracts the benefits of dietary restriction in old mice. Nature Metabolism 1, 1–29 (2019).
13. Lumeng CN et al. Aging is associated with an increase in T cells and inflammatory macrophages in visceral adipose tissue. The Journal of Immunology 187, 6208–6216 (2011). [PubMed: 22075699]
14. Rosenberg HF, Dyer KD & Foster PS Eosinophils: changing perspectives in health and disease. Nat Rev Immunol 13, 9–22 (2013). [PubMed: 23154224]
15. Wu D et al. Eosinophils sustain adipose alternatively activated macrophages associated with glucose homeostasis. Science 332, 243–247 (2011). [PubMed: 21436399]
16. Lackey DE & Olefsky JM Regulation of metabolism by the innate immune system. Nat Rev Endocrinol 12, 15–28 (2016). [PubMed: 26553134]

17. Pérez LM et al. 'Adipaging': ageing and obesity share biological hallmarks related to a dysfunctional adipose tissue. J. Physiol. (Lond.) 594, 3187–3207 (2016). [PubMed: 26926488]
18. Villeda SA et al. The ageing systemic milieu negatively regulates neurogenesis and cognitive function. Nature 477, 90–94 (2011). [PubMed: 21886162]
19. Franceschi C & Campisi J Chronic inflammation (inflammaging) and its potential contribution to age-associated diseases. J Gerontol A Biol Sci Med Sci 69 Suppl 1, S4–9 (2014). [PubMed: 24833586]
20. Furman D et al. Chronic inflammation in the etiology of disease across the life span. Nat Med 25, 1–11 (2019). [PubMed: 30617338]
21. Tabula Muris Consortium et al. Single-cell transcriptomics of 20 mouse organs creates a Tabula Muris. Nature 562, 367–372 (2018). [PubMed: 30283141]
22. Villeda SA et al. Young blood reverses age-related impairments in cognitive function and synaptic plasticity in mice. Nat Med 20, 659–663 (2014). [PubMed: 24793238]
23. Conboy IM et al. Rejuvenation of aged progenitor cells by exposure to a young systemic environment. Nature 433, 760–764 (2005). [PubMed: 15716955]
24. Katsimpardi L et al. Vascular and neurogenic rejuvenation of the aging mouse brain by young systemic factors. Science 344, 630–634 (2014). [PubMed: 24797482]
25. Loffredo FS et al. Growth Differentiation Factor 11 Is a Circulating Factor that Reverses Age-Related Cardiac Hypertrophy. Cell 153, 828–839 (2013). [PubMed: 23663781]
26. Baht GS et al. Exposure to a youthful circulaton rejuvenates bone repair through modulation of β-catenin. Nat Commun 6, 7131 (2015). [PubMed: 25988592]
27. Ruckh JM et al. Rejuvenation of Regeneration in the Aging Central Nervous System. Stem Cell 10, 96–103 (2012).
28. Eggel A & Wyss-Coray T A revival of parabiosis in biomedical research. Swiss Med Wkly 144, w13914 (2014). [PubMed: 24496774]
29. Lee M-W et al. Activated type 2 innate lymphoid cells regulate beige fat biogenesis. Cell 160, 74–87 (2015). [PubMed: 25543153]
30. Qiu Y et al. Eosinophils and type 2 cytokine signaling in macrophages orchestrate development of functional beige fat. Cell 157, 1292–1308 (2014). [PubMed: 24906148]
31. Lee NA et al. Expression of IL-5 in thymocytes/T cells leads to the development of a massive eosinophilia, extramedullary eosinophilopoiesis, and unique histopathologies. J Immunol 158, 1332–1344 (1997). [PubMed: 9013977]
32. Conboy IM, Conboy MJ, Smythe GM & Rando TA Notch-mediated restoration of regenerative potential to aged muscle. Science 302, 1575–1577 (2003). [PubMed: 14645852]
33. Shefer G, Van de Mark DP, Richardson JB & Yablonka-Reuveni Z Satellite-cell pool size does matter: defining the myogenic potency of aging skeletal muscle. Dev Biol 294, 50–66 (2006). [PubMed: 16554047]
34. Fairfax KA et al. Transcriptional profiling of eosinophil subsets in interleukin-5 transgenic mice. J Leukoc Biol 104, 195–204 (2018). [PubMed: 29758105]
35. Ohnmacht C, Pullner A, van Rooijen N & Voehringer D Analysis of eosinophil turnover in vivo reveals their active recruitment to and prolonged survival in the peritoneal cavity. J Immunol 179, 4766–4774 (2007). [PubMed: 17878375]
36. Sudo K, Ema H, Morita Y & Nakauchi H Age-associated characteristics of murine hematopoietic stem cells. J Exp Med 192, 1273–1280 (2000). [PubMed: 11067876]
37. de Haan G & Van Zant G Dynamic changes in mouse hematopoietic stem cell numbers during aging. Blood 93, 3294–3301 (1999). [PubMed: 10233881]
38. Reynaud D et al. IL-6 controls leukemic multipotent progenitor cell fate and contributes to chronic myelogenous leukemia development. Cancer Cell 20, 661–673 (2011). [PubMed: 22094259]
39. Riether C, Schürch CM & Ochsenbein AF Regulation of hematopoietic and leukemic stem cells by the immune system. Cell Death Differ 22, 187–198 (2015). [PubMed: 24992931]
40. Schürch CM, Riether C & Ochsenbein AF Cytotoxic CD8+ T cells stimulate hematopoietic progenitors by promoting cytokine release from bone marrow mesenchymal stromal cells. Cell Stem Cell 14, 460–472 (2014). [PubMed: 24561082]

41. Pioli PD, Casero D, Montecino-Rodriguez E, Morrison SL & Dorshkind K Plasma Cells Are Obligate Effectors of Enhanced Myelopoiesis in Aging Bone Marrow. Immunity 1–23 (2019). doi:10.1016/j.immuni.2019.06.006
42. Akunuru S & Geiger H Aging, Clonality, and Rejuvenation of Hematopoietic Stem Cells. Trends in Molecular Medicine 22, 701–712 (2016). [PubMed: 27380967]
43. Geiger H, de Haan G & Florian MC The ageing haematopoietic stem cell compartment. Nat Rev Immunol 13, 376–389 (2013). [PubMed: 23584423]
44. Shaw AC, Joshi S, Greenwood H, Panda A & Lord JM Aging of the innate immune system. Curr Opin Immunol 22, 507–513 (2010). [PubMed: 20667703]
45. Goronzy JJ & Weyand CM Understanding immunosenescence to improve responses to vaccines. Nature Publishing Group 14, 428–436 (2013).
46. Salvioli S et al. Inflamm-aging, cytokines and aging: state of the art, new hypotheses on the role of mitochondria and new perspectives from systems biology. Current pharmaceutical design 12, 3161–3171 (2006). [PubMed: 16918441]
47. Zwick RK, Guerrero-Juarez CF, Horsley V & Plikus MV Anatomical, Physiological, and Functional Diversity of Adipose Tissue. Cell Metabolism 27, 68–83 (2018). [PubMed: 29320711]
48. Zoico E et al. Brown and Beige Adipose Tissue and Aging. Front Endocrinol (Lausanne) 10, 1194 (2019).
49. Ghosh AK, O'Brien M, Mau T, Qi N & Yung R Adipose Tissue Senescence and Inflammation in Aging is Reversed by the Young Milieu. J Gerontol A Biol Sci Med Sci 74, 1709–1715 (2019). [PubMed: 30590424]
50. Yu P, Yuan R, Yang X & Qi Z Adipose tissue, aging, and metabolism. Current Opinion in Endocrine and Metabolic Research 5, 11–20 (2019).
51. Wu D et al. Aging up-regulates expression of inflammatory mediators in mouse adipose tissue. The Journal of Immunology 179, 4829 (2007). [PubMed: 17878382]
52. Franceschi C, Garagnani P, Vitale G, Capri M & Salvioli S Inflammaging and 'Garb-aging'. Trends in Endocrinology & Metabolism 28, 199–212 (2017). [PubMed: 27789101]
53. Kusminski CM, Bickel PE & Scherer PE Targeting adipose tissue in the treatment of obesity-associated diabetes. Nat Rev Drug Discov 15, 639–660 (2016). [PubMed: 27256476]
54. Starr ME, Saito M, Evers BM & Saito H Age-Associated Increase in Cytokine Production During Systemic Inflammation—II: The Role of IL-1β in Age-Dependent IL-6 Upregulation in Adipose Tissue. J Gerontol A Biol Sci Med Sci 70, 1508–1515 (2015). [PubMed: 25344820]
55. Soysal P et al. Inflammation and frailty in the elderly: A systematic review and meta-analysis. Ageing Res. Rev 31, 1–8 (2016). [PubMed: 27592340]
56. Oh J, Lee YD & Wagers AJ Stem cell aging: mechanisms, regulators and therapeutic opportunities. Nat Med 20, 870–880 (2014). [PubMed: 25100532]
57. Geiger H & Van Zant G The aging of lympho-hematopoietic stem cells. Nat Immunol 3, 329–333 (2002). [PubMed: 11919569]
58. Vogelaar CF et al. Fast direct neuronal signaling via the IL-4 receptor as therapeutic target in neuroinflammation. Sci Transl Med 10, eaao2304 (2018). [PubMed: 29491183]
59. Schneider CA, Rasband WS & Eliceiri KW NIH Image to ImageJ: 25 years of image analysis. Nat Meth 9, 671–675 (2012).
60. Liu L, Cheung TH, Charville GW & Rando TA Isolation of skeletal muscle stem cells by fluorescence-activated cell sorting. Nature protocols 10, 1612–1624 (2015). [PubMed: 26401916]
61. Dyer KD et al. Functionally competent eosinophils differentiated ex vivo in high purity from normal mouse bone marrow. The Journal of Immunology 181, 4004–4009 (2008). [PubMed: 18768855]
62. Zhang H et al. NAD+ repletion improves mitochondrial and stem cell function and enhances life span in mice. Science 352, aaf2693–1443 (2016).
63. R Core Team. R: A Language and Environment for Statistical Computing. (2014).
64. van den Berg RA, Hoefsloot HCJ, Westerhuis JA, Smilde AK & van der Werf MJ Centering, scaling, and transformations: improving the biological information content of metabolomics data. BMC Genomics 7, 142 (2006). [PubMed: 16762068]

65. de Hoon MJL, Imoto S, Nolan J & Miyano S Open source clustering software. Bioinformatics 20, 1453–1454 (2004). [PubMed: 14871861]

66. Saldanha AJ Java Treeview--extensible visualization of microarray data. Bioinformatics 20, 3246–3248 (2004). [PubMed: 15180930]

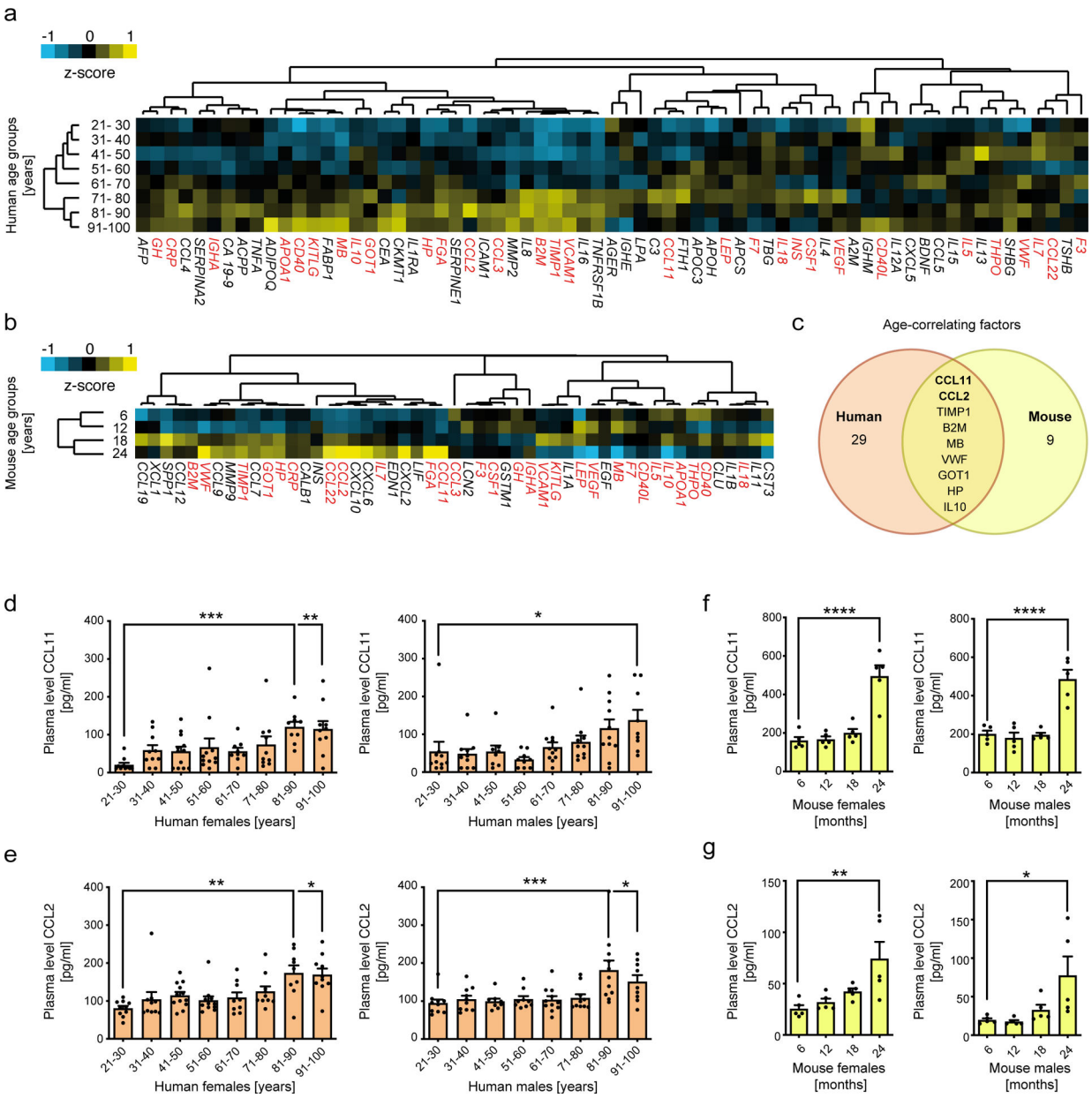

Fig. 1. Age-related changes in the plasma proteome of humans and mice.

Unsupervised clustering of different age groups (humans n=20 per group; mice n=10 per group) based on the levels of 67 human plasma factors (a) and 40 mouse plasma factors (b). Means of z-scored values were used for clustering and are displayed as color code ranging from blue (negative) to yellow (positive). Each factor is denominated with its official HUGO gene nomenclature. Red labels indicate factors that were detectable in both human and mouse cohorts. (c) Venn diagram representing plasma factors significantly correlating with age in humans (n=160 biologically independent donors) and mice (n=40). Sex-specific protein levels of (d) CCL11 and (e) CCL2 in human plasma (n=10 per group). (f) CCL11 and (g) CCL2 plasma levels in male and female mice (n=5 per group) of indicated age groups. Correlations between plasma factor level and age were calculated using Pearsons'r.

Statistical significance was calculated by one-way ANOVA followed by two-tailed post-hoc Dunnett`s multiple comparison against the youngest group. Wherever possible, data are shown as individual data points with mean ± SEM. *$p < 0.05$, **$p < 0.01$, ***$p < 0.001$.

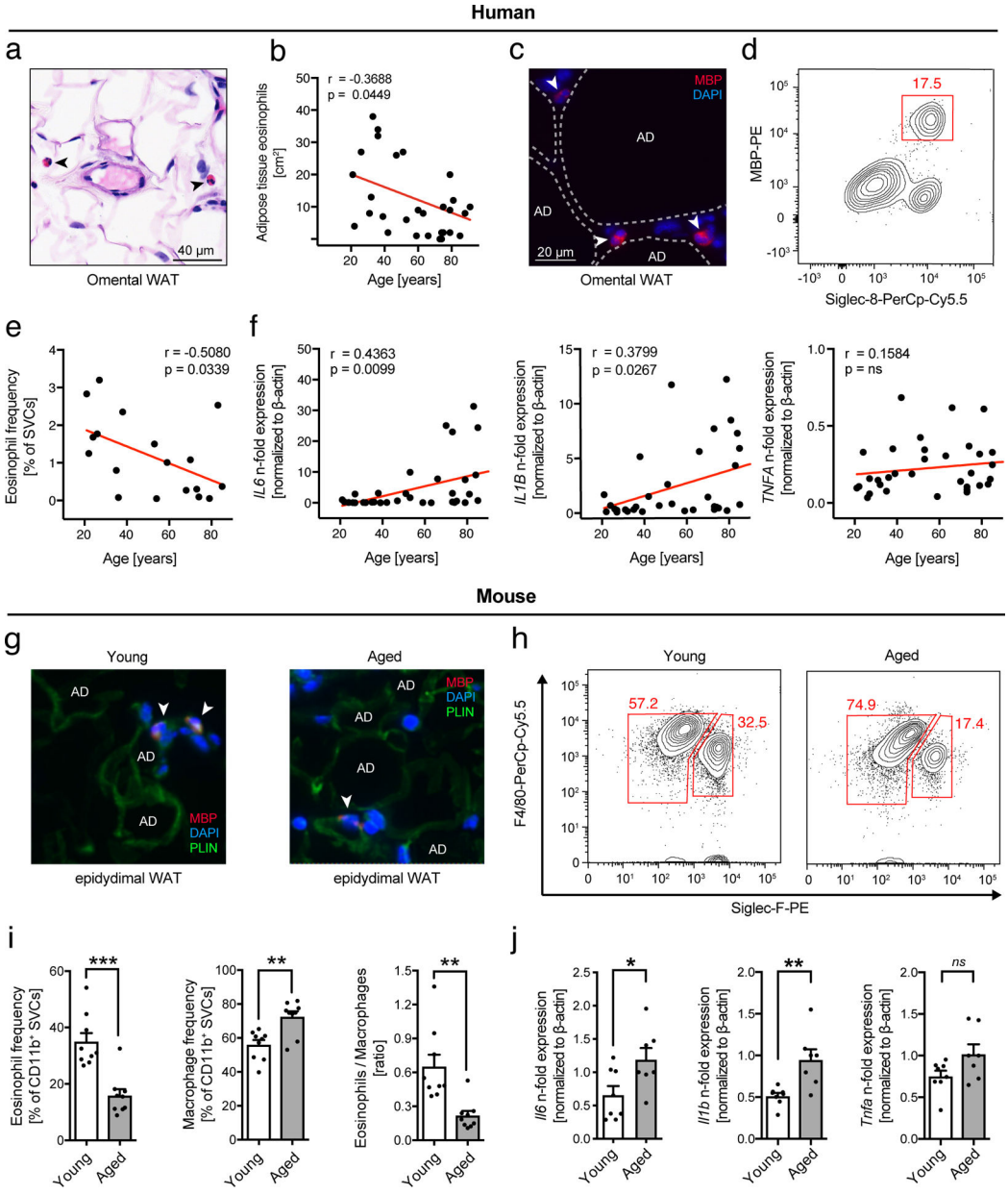

Fig. 2. Age-related changes in innate immune cell distribution in WAT of human and mice.

(a) Representative image of H&E stained human omental adipose tissue. Arrows point to eosinophils. Scale bar: 40 µm. (b) Quantification of tissue-resident eosinophils in H&E stained sections of human omental adipose tissues (n=30 biologically independent human donors). (c) Representative images of major basic protein (MBP)-stained human omental adipose tissue. Arrows point towards MBP-positive eosinophils. One out of three independently performed experiments is shown. (d) Representative flow plots of MBP- and Siglec-8 positive eosinophils and (e) corresponding quantification of eosinophil frequencies in the stromal vascular cell (SVC) fraction of human omental adipose tissue (n=18 biologically independent human donors). (f) Fold induction of *Tnfa*, *Il1β and Il6* mRNA expression levels in human omental adipose tissue (n=34 biologically independent human

donors). (g) Representative images of major basic protein (MBP)-stained mouse epididymal WAT. Arrows point towards MBP-positive eosinophils. Adipocytes are stained for perilipin (PLIN). One out of three independently performed experiments is shown. (h) Representative flow plots of adipose tissue macrophage ATM (F4/80^{+}, SiglecF^{-}) and ATE (F4/80^{int}, SiglecF^{+}) populations in eWAT from young (3 months) and aged (20 months) mice. (i) Frequencies of eosinophils and macrophages and calculated eosinophil:macrophage ratio in eWAT of young and aged mice (n=9 per group). (j) Fold induction of *Tnfa*, *Il1β and Il6* mRNA expression levels in eWAT of young (n=8) and aged mice (n=7). Data are presented as fold expression over aged mice and pooled from two independently performed experiments. Statistical significance was calculated by unpaired two-tailed Student's t test (i, j) or the Pearson correlation coefficient between eosinophils and age (b, e) or fold gene expression levels and age (f) is given. Results are shown as individual data points with mean ± SEM. *$p < 0.05$, **$p < 0.01$, ***$p < 0.001$.

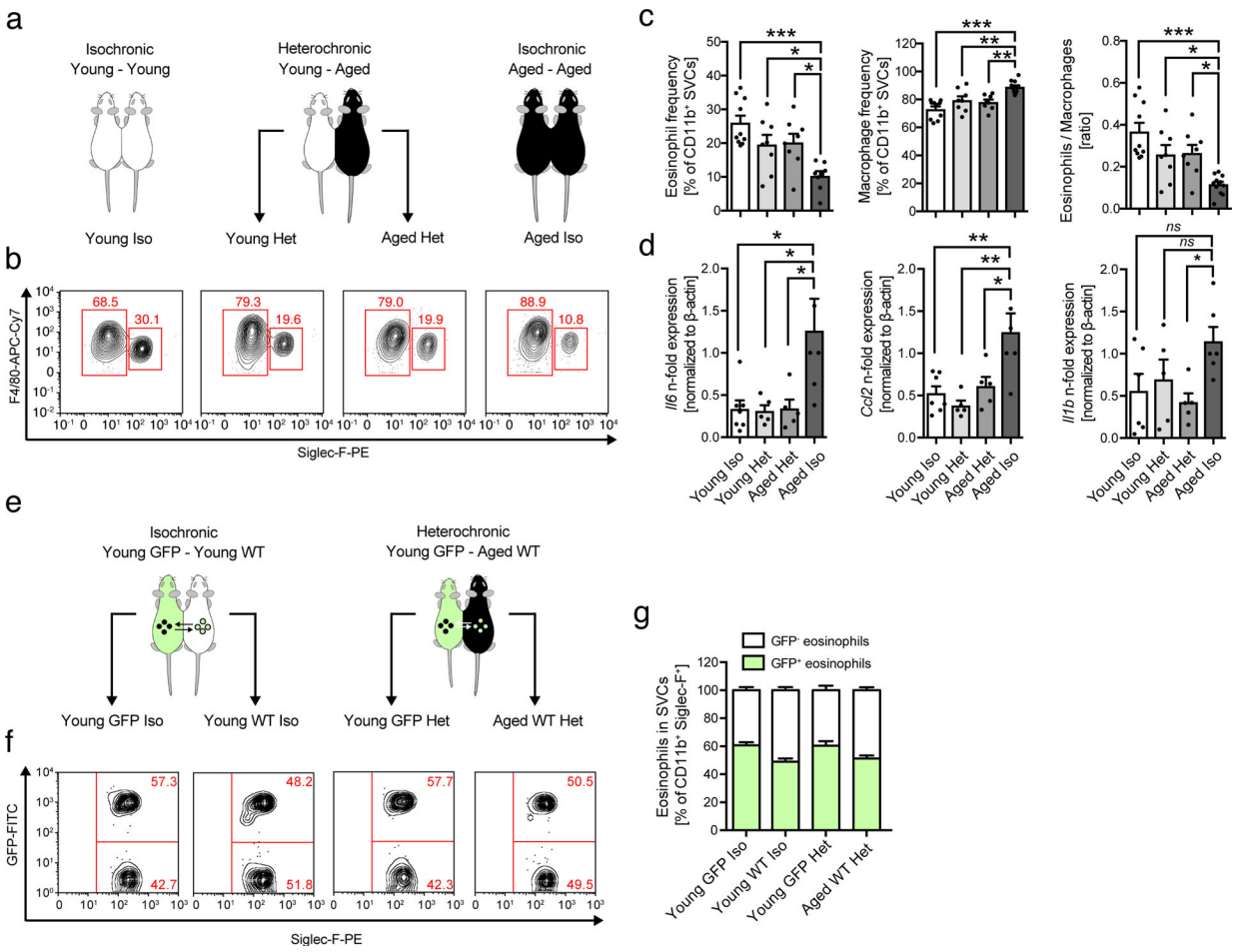

Fig. 3. Heterochronic parabiosis restores ATE:ATM ratios and limits WAT inflammation

(a) Experimental protocol. (b) Representative flow plots of ATE (F4/80^{int}, SiglecF^{+}) and ATM (F4/80^{+}, SiglecF^{-}) populations in eWAT of iso- and heterochronic parabionts. (c) Frequencies of ATEs and ATMs and the calculated ATE:ATM ratios from two independently performed and pooled experiments in eWAT of parabiosed mice (young isochronic, n=10; young heterochronic, n=8; old heterochronic, n=8; old isochronic, n=12). (d) mRNA expression levels for *Il6, Ccl2* (young isochronic, n=7; young heterochronic, n=5; old heterochronic, n=5; old isochronic, n=6) and *Il1β* (young isochronic, n=6; young heterochronic, n=5; old heterochronic, n=5; old isochronic, n=6), in eWAT of parabiosed mice. Data are presented as fold expression over old isochronic controls and pooled from two independently performed experiments. (e) Experimental protocol. Isochronic and heterochronic parabiosis was performed by joining young (2–3 months) GFP-reporter mice (GFP) to either young (2–3 months) or aged (18 months) wild-type C57BL/6 mice. (f) Representative flow plots of GFP^{+} and GFP^{-} eosinophils in WAT of isochronic or heterochronic parabionts. (g) Percentages of GFP^{+} and GFP^{-} eosinophils in WAT of Young GFP Iso (n=5), Young GFP Het (n=5), Young WT Iso (n=5), and Aged WT Het mice (n=5). The experiment was done once. Statistical significance was calculated by one-way ANOVA followed by two-tailed post-hoc Dunnett's multiple comparison test against the aged

isochronic group (c,d). Wherever possible, data are shown as individual data points with mean ± SEM. *$p < 0.05$, **$p < 0.01$, ***$p < 0.001$.

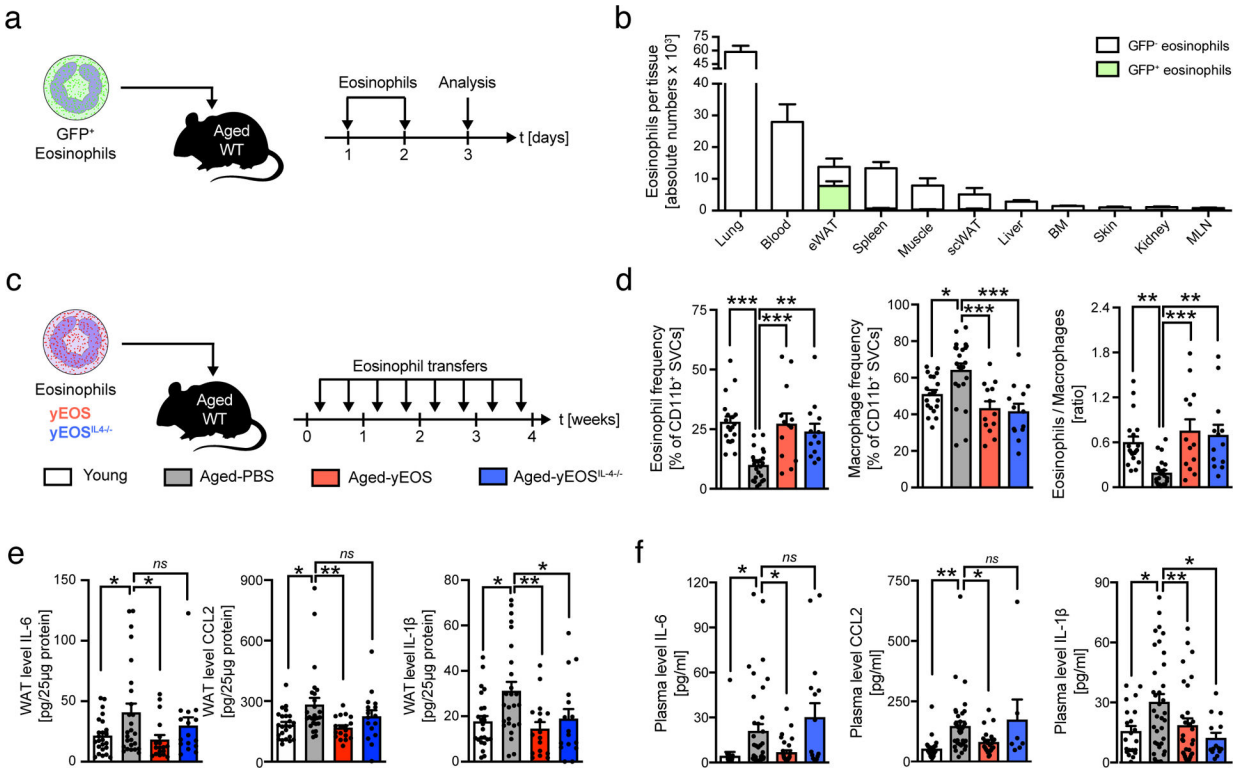

Figure 4. Transfer of eosinophils from young donors reverse aging signatures in WAT and limits systemic inflammation.

Aged mice (18 months) were adoptively transferred with sort-purified GFP$^+$ eosinophils on two subsequent days. The following day eosinophil recruitment into different tissues was assessed by flow cytometry. (a) Representative flow plots of transferred GFP$^+$ and resident GFP$^-$ eosinophils in indicated tissues. (b) Number of GFP$^+$ and GFP$^-$ resident eosinophils in indicated tissues. Data are representative of n=4 per group. One out of two independently performed experiments is shown. (c) Experimental protocol. (d) Frequencies of ATEs and ATMs and the calculated ATE:ATM ratios in eWAT of young (n=19), Aged-PBS (n=23), Aged-yEOS (n=13) and Aged-yEOS$^{IL-4-/-}$ (n=13) mice. (e) Protein levels in eWAT of young (n=24), Aged-PBS (n=26), Aged-yEOS (n=18) and Aged-yEOS$^{IL-4-/-}$ (n=16) mice. (f) Plasma protein levels for IL-6 and IL-1β in young (n=20), Aged-PBS (n=35), Aged-yEOS (n=32) and Aged-yEOS$^{IL-4-/-}$ (n=14) mice and CCL2 plasma protein levels in young (n=26), Aged-PBS (n=37), Aged-yEOS (n=22) and Aged-yEOS$^{IL-4-/-}$ (n=7) mice. Statistical significance was calculated by one-way ANOVA followed by two-tailed post-hoc Dunnett's multiple comparison test against the Aged-PBS group (d, e, f) and wherever possible, results are shown as individual data points with mean bars ± SEM. *$p < 0.05$, **$p < 0.01$, ***$p < 0.001$.

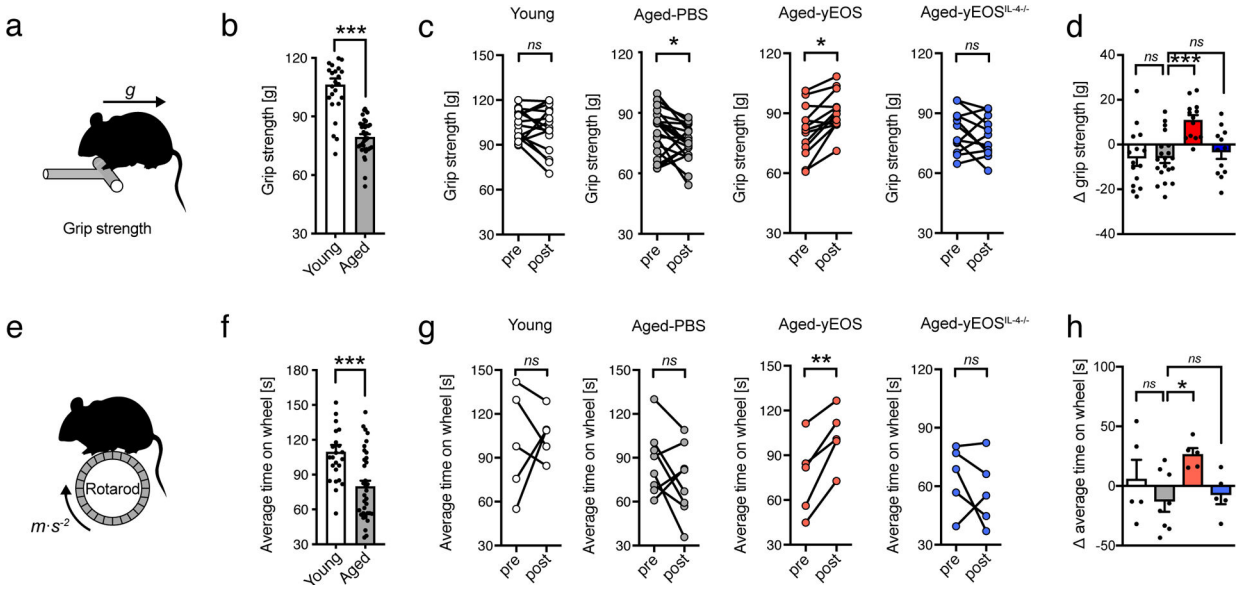

Figure 5. Eosinophils from young donors improve physical fitness in aged hosts.

(a) Schematic grip strength test. (b) Age-related changes in physical performance in young (3 months, n=24) and aged mice (20 months, n=35). (c) Intra- and (d) inter-group comparisons of maximal force (grip strength) of young (n=15), Aged-PBS (n=18), Aged-yEOS (n=13) and Aged-yEOS$^{IL-4-/-}$ (n=12) mice. Pooled data from two independently performed experiments are shown. (e) Schematic of Rotarod test. (f) Age-related changes in physical performance in young (3 months, n=25) and aged mice (20 months, n=35). (g) Intra- and (h) inter-group comparison of average time on wheel (Rotarod test) of young (n=5), Aged-PBS (n=8), Aged-yEOS (n=5) and Aged-yEOS$^{IL-4-/-}$ (n=5) mice. The experiment (g, h) was done once. Delta in performances in (d) and (h) are calculated relative to baseline (post- minus pre-treatment results). Statistical significance was calculated by unpaired two-tailed Student's t test (b, f,), Wilcoxon matched pairs signed rank test (c, g) or one-way ANOVA followed by two-tailed post-hoc Dunnett's multiple comparison test against the aged-PBS treated group (d, h). Data are shown as individual data points with mean bars ± SEM. *p < 0.05, **p < 0.01, ***p < 0.001.

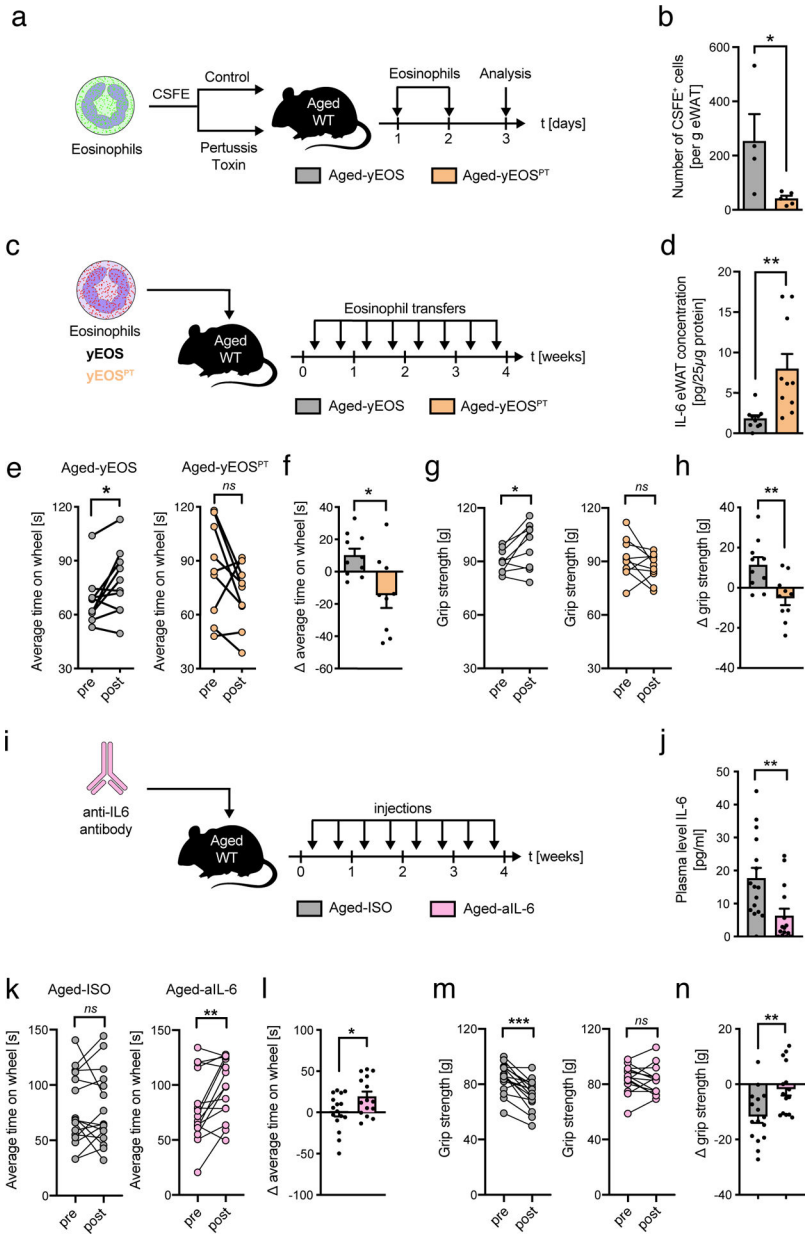

Fig. 6. Eosinophil homing to WAT lowers age-related adipose tissue inflammation and improves physical fitness in aged recipients.

(a) Experimental protocol. (b) Number of CSFE-labeled eosinophils in eWAT of control treated Aged-yEOS (n=4) and PT pre-treated Aged-yEOS^{PT} mice (n=5) as measured by flow cytometry. One out of two independently performed experiments is shown. (c) Experimental protocol. (d) eWAT IL-6 protein levels in Aged-PBS (n=10) and Aged-yEOS^{PT} (n=10) mice. (e) Intra- and inter-group (f) comparison of average time on wheel (Rotarod test) of Aged-yEOS (n=10) and Aged-yEOS^{PT} (n=10) mice. (g) Intra- and inter-group (h) comparison of maximal force (grip strength) of Aged-yEos (n=10) and Aged-yEOS^{PT} (n=10) mice. Delta in performances for (f) and (h) were calculated relative to baseline (post- minus pre-treatment results). The experiment (c-h) was done once. (i) Experimental protocol. (j) IL-6 plasma levels relative to baseline (pre-treatment) in Aged-

ISO (n=16) and Aged-aIL6 (n=15) mice. (k) Intra- and inter-group (l) comparison of average time on wheel (Rotarod test) of Aged-PBS (n=16) and Aged-aIL6 (n=15) mice. (m) Intra- and inter-group (n) comparison of maximal force (grip strength) of Aged-PBS (n=16) and Aged-aIL6 (n=15) mice. Delta in performance was calculated relative to baseline (post-minus pre-treatment results). Data (i-n) are pooled from two independently performed experiments. Statistical significance was calculated by Wilcoxon matched pairs signed rank test (e, g, k, m) or by unpaired two-tailed Student's *t* test (b, d, f, h, j, l, n) and data are shown as individual data points with mean ± SEM. ns: not significant, *p < 0.05, **p < 0.01, ***p < 0.001.

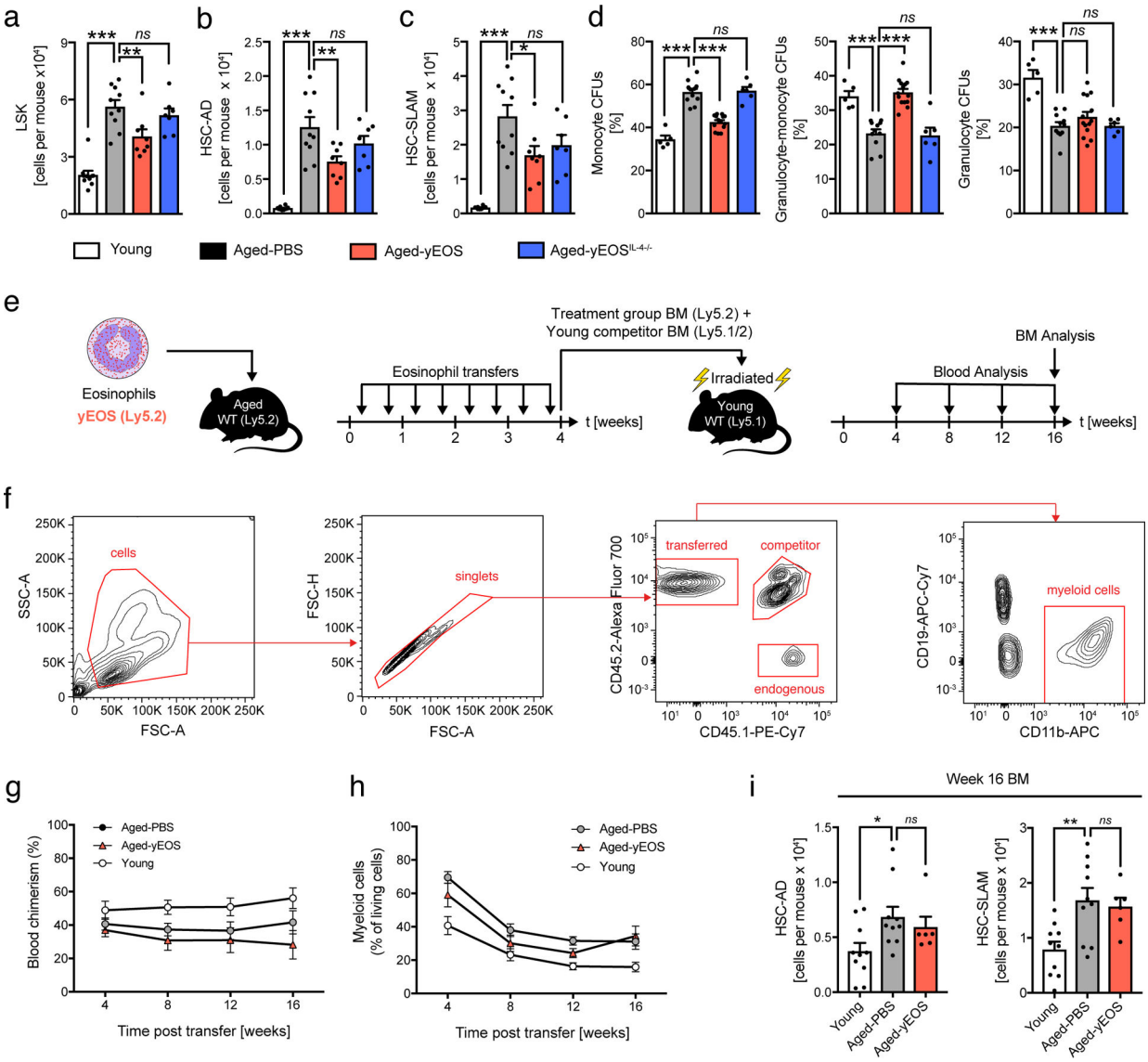

Fig. 7. Transfer of eosinophils into aged mice transiently alters hematopoietic stem cell numbers and age-related myeloid skewing

(a) Absolute numbers of Lin$^-$, Sca-1$^+$, c-kit$^+$ hematopoietic stem cells (LSKs) in young (n=10), Aged-PBS (n=10), Aged-yEOS (n=8) and Aged-yEOS$^{IL-4-/-}$ (n=7) mice. Quantification of HSCs using CD34 and FLT3 (b) or SLAM markers (c) in indicated groups. (d) Quantification of the percentage of monocyte colony phenotypes in plated Lin$^-$ BM methylcellulose cultures of young (n=5), Aged-PBS (n=11), Aged-yEOS (n=14) and Aged-yEOS$^{IL-4-/-}$ (n=6) mice. Data (a-d) are pooled from two independently performed experiments (e) Model of transplantation (f) Representative gating strategy to discriminate peripheral blood donor from competitor and endogenous myeloid cells. (g) Blood chimerism of Young (n=10), Aged-PBS (n=10) and Aged-yEOS mice (n=6) mice. (h) Frequencies of blood myeloid cells of Young (n=10), Aged-PBS (n=10) and Aged-yEOS mice (n=6) mice at indicated timepoints. (i) Absolute numbers of HSC-AD and HSC-SLAM cells in Young (n=10), Aged-PBS (n=10) and Aged-yEOS mice (n=6) mice 16 weeks post bone marrow

transplant. The experiment (f-i) was done once. Statistical significance was calculated by one-way ANOVA followed by two-tailed post-hoc Dunnett's multiple comparison test against the aged-PBS treated group. Data are shown as individual data points with mean ± SEM. *$p < 0.05$, **$p < 0.01$, ***$p < 0.001$.

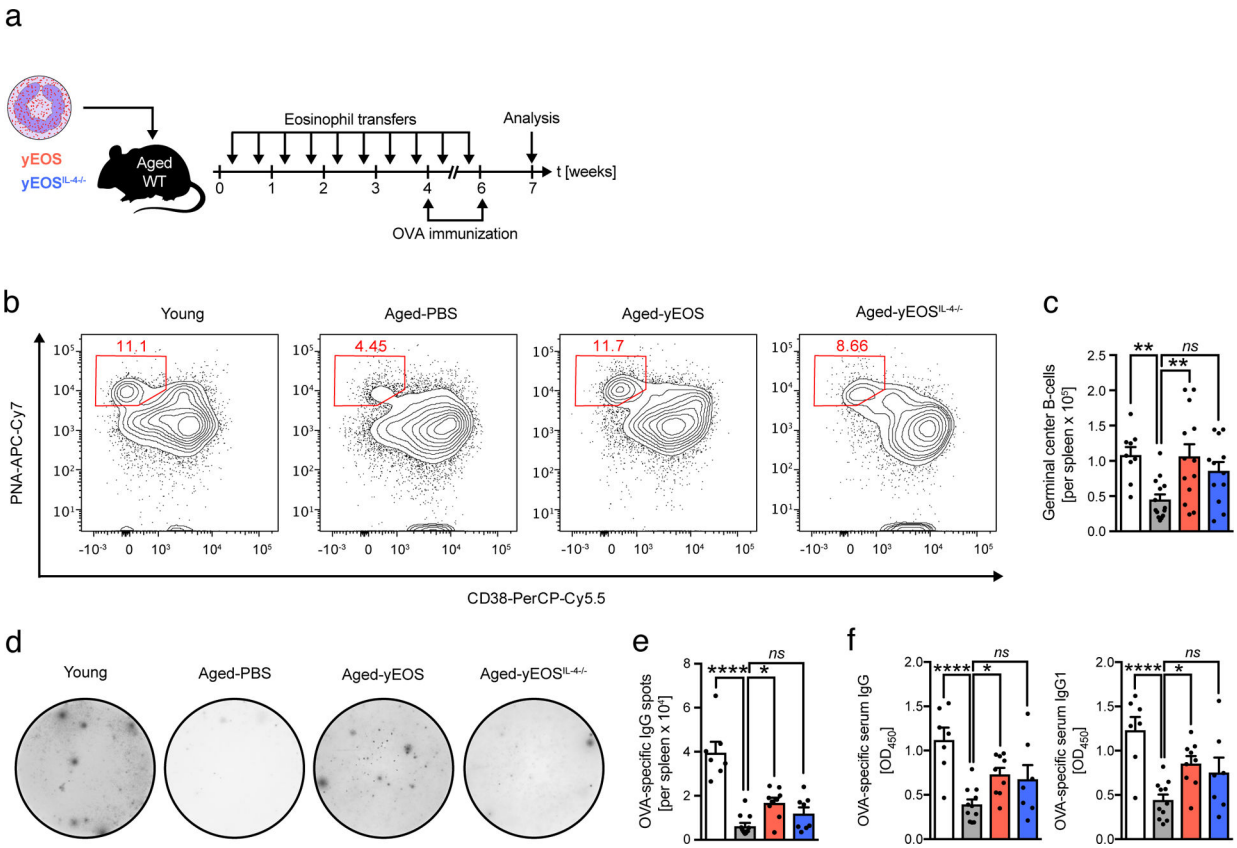

Fig. 8. Transfer of eosinophils into aged mice is associated with improved immunological fitness.

(a) Immunization protocol. (b) Representative flow plots of germinal center B cell (PNA^+, $CD38^-$) populations in spleens of indicated groups. (c) Total numbers of germinal center B cells in young (*n*=9), Aged-PBS (*n*=14), Aged-yEOS (*n*=13) and Aged-yEOS$^{IL-4-/-}$ (*n*=12) mice. (d) Representative photographs and (e) quantification of OVA-specific IgG immunospots derived from splenocyte cultures of young (*n*=7), Aged-PBS (*n*=11), Aged-yEOS (*n*=9) and Aged-yEOS$^{IL-4-/-}$ (*n*=7) mice. (f) Quantification of OVA-specific serum IgG and IgG1 of young (*n*=7), Aged-PBS (*n*=11), Aged-yEOS (*n*=9) and Aged-yEOS$^{IL-4-/-}$ (*n*=7) mice. Data (b-f) are pooled from two independently performed experiments. Statistical significance was calculated by one-way ANOVA followed by two-tailed post-hoc Dunnett's multiple comparison test against the aged-PBS treated group. Data are shown as individual data points with mean ± SEM. *p < 0.05, **p < 0.01, ***p < 0.001.

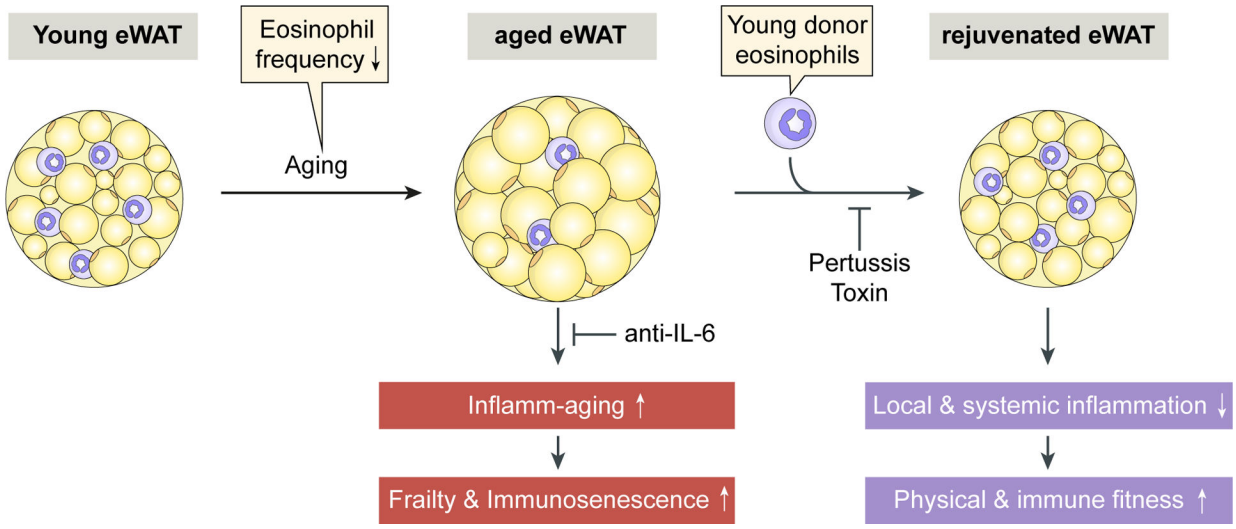

Fig 9. Schematic representation illustrating the rejuvenating potential of young donor eosinophils in aged hosts.

The age-related decrease of eosinophil frequency in epididymal white adipose tissue (eWAT) is associate with the occurrence of inflamm-aging, frailty and immunosenescence. Our study demonstrates that these aging phenotypes are reversible upon young donor eosinophil transfers which dampen local and systemic inflammation leading to improved physical and immune fitness. The observed rejuvenation of the aged host upon young donor eosinophil transfers is dependent on their migration into eWAT since pertussis toxin treatment of the cells abrogates these effects. Systemic blocking of IL-6 only partially phenocopies physical improvements observed upon transfer of eosinophils.